



Minerva Access is the Institutional Repository of The University of Melbourne

Author/s:

Warren, RA;Jakob, C;Hitchcock, SM;White, BA

Title:

Heavy versus extreme rainfall events in southeast Australia

Date:

2021-07-01

Citation:

Warren, R. A., Jakob, C., Hitchcock, S. M. & White, B. A. (2021). Heavy versus extreme rainfall events in southeast Australia. *Quarterly Journal of the Royal Meteorological Society*, 147 (739), pp.3201-3226. <https://doi.org/10.1002/qj.4124>.

Persistent Link:

<https://hdl.handle.net/11343/298839>

2

3 Heavy versus extreme rainfall events in southeast 4 Australia

5 Robert A. Warren^{1,2} | Christian Jakob^{1,2} | Stacey M.
Hitchcock^{2,3} | Bethan A. White^{1,2}

¹School of Earth, Atmosphere and Environment, Monash University, Clayton, Victoria, Australia

²Australian Research Council Centre of Excellence for Climate Extremes, Melbourne, Victoria, Australia

³School of Earth Sciences, University of Melbourne, Parkville, Victoria, Australia

Correspondence

R. A. Warren, Weather and Environmental Prediction Program, Bureau of Meteorology, Melbourne, Victoria, Australia
Email: rob.warren1@bom.gov.au

Funding information

Australian Research Council, CE170100023

Focussing on the major cities of Brisbane, Sydney, and Melbourne in south-east Australia, this study seeks to determine the environmental factors that distinguish between *heavy* rainfall events (HREs) and *extreme* rainfall events (EREs). Using daily rain gauge observations, HREs and EREs are defined for each domain based, respectively, on the 95th and 99th percentiles of wet-day rainfall for the period 1979–2018. K-means clustering is applied to mean sea-level pressure data from ERA5 to obtain a set of representative large-scale circulation patterns associated with these events. Composite synoptic maps, mean vertical profiles, and a series of column-integrated diagnostics are then examined for each cluster and used to compare the environmental characteristics of HREs and EREs. For all three cities, HREs are associated with an upper-level trough to the west, with large-scale ascent, positive column water vapour (CWV) anomalies, and strong moisture transport over the analysis domain. For Brisbane and Sydney on the east coast, the clusters are characterised by a coastal trough/low with moist onshore flow from the Tasman and Coral Seas. For Melbourne, circulation patterns are more distinct, with clusters characterised by a front, a cut-off low, and an inland trough. Compared to HREs, EREs show a more amplified upper-level trough, with stronger vertical motion and larger CWV anomalies over the analysis domain. In Brisbane and Sydney, EREs also feature stronger and deeper onshore flow, promoting enhanced moisture transport. A diagnostic termed upward vapour transport, which combines the key ingredients of high CWV and large-scale ascent, is shown to discriminate well between HREs and EREs in all three domains. In contrast, surface temperature, which is frequently linked to rainfall extremes via Clausius–Clapeyron scaling, shows significant overlap between the different event categories, particularly for Brisbane and Sydney.

Keywords — precipitation extremes, large-scale circulation, cluster analysis

1 INTRODUCTION

In her poem *My Country*, Dorothea Mackellar (1885–1968) memorably describes Australia as a land “of droughts and flooding rains”. It is an apt characterisation when we consider the significant spatial and temporal variations in precipitation observed across the continent. Rainfall is generally plentiful and distributed throughout the year in the southeast, substantial but seasonal in the southwest and tropical north, and highly irregular in the arid interior. In much of Australia, precipitation is also subject to large interannual variability (Nicholls et al., 1997). This in part reflects the strong influence of large-scale modes of variability, such as the El Niño–Southern Oscillation (ENSO), Indian Ocean dipole, and southern annular mode (Risbey et al., 2009). These modes have been found to influence not only average seasonal rainfall, but also rainfall extremes (Min et al., 2013; King et al., 2014), suggesting the potential for long-range predictions of these high-impact events (King et al., 2020). However, on daily timescales the occurrence of localised extreme precipitation is primarily driven by synoptic-scale circulations, which supply the ingredients required for intense rainfall. Furthermore, recent work suggests that the statistical association between modes of variability, such as ENSO, and Australian rainfall is realised via changes in the relative frequency of different circulation types (Hauser et al., 2020). An improved understanding of the synoptic-scale drivers of extreme rainfall can therefore contribute to better prediction of these events across a wide range of timescales. This knowledge can also be used to inform future projections of extreme rainfall, via the application of statistical downscaling techniques (e.g. Rau et al., 2020).

Investigations into the synoptic-scale drivers of local high-impact weather events typically follow one of two approaches. The first involves the identification of relevant dynamical features, which are then linked to the phenomenon of interest based on spatial and temporal proximity criteria. In the context of precipitation extremes, these dynamical features include tropical cyclones (e.g. Knight and Davis, 2009; Villarini and Denniston, 2016; Zhang et al., 2018), midlatitude cyclones and fronts (e.g. Pfahl and Wernli, 2012; Catto and Pfahl, 2013; Dowdy and Catto, 2017), atmospheric rivers (e.g. Ralph et al., 2006; Lavers et al., 2011; Kamae et al., 2017), and potential vorticity streamers (e.g. Martius et al., 2006; de Vries et al., 2018; Moore et al., 2019). In Australia, studies following this *feature-based approach* have highlighted the dominant contribution of extratropical cyclones and fronts to daily and subdaily precipitation extremes in the south of the country (Catto and Pfahl, 2013; Dowdy and Catto, 2017; Utsumi et al., 2017; Pepler et al., 2020), with the frequent co-occurrence of thunderstorms (Dowdy and Catto, 2017) or conditions conducive to thunderstorms (Pepler et al., 2020) suggesting that the associated rainfall systems are often convective in nature. Tropical cyclones contribute significantly to extreme daily and multiday rainfall totals in the north of the country, particularly along the northern coast of Western Australia (Villarini and Denniston, 2016), while along the eastern seaboard so-called east coast lows (ECLs) account for the majority of wintertime heavy rainfall days (Pepler et al., 2014). The northwest cloudband has also been shown to enhance the probability of extreme precipitation in northwest, central, and southeast Australia (Reid et al., 2019).

The second approach to investigating synoptic-scale drivers of local high-impact weather events considers the large-scale circulation patterns (LSCPs) (sometimes referred to as weather patterns or weather types) associated with these events. In its most basic form, this can simply involve the compositing of relevant fields across all event days; however, results may be misleading if these days encompass multiple distinct LSCPs. As such it is common to employ an intermediate step where events are grouped based on the characteristics of the associated synoptic environment. This process can be performed manually by an experienced analyst or using automated methods such as K-means clustering, principal component analysis, or self-organising maps. This *pattern-based approach* has been used to investigate synoptic-scale environments associated with extreme precipitation in many parts of the world, including the United States (Maddox et al., 1979; Konrad, 1997; Swales et al., 2016), China (Chen and Zhai, 2014; Huang et al., 2018; Hu et al., 2019), southern Europe (Houssos et al., 2008; Nuissier et al., 2011; Grazzini et al., 2020), the United Kingdom (Champion et al., 2019; Allan et al., 2019), and Japan (Ohba et al., 2015). The approach has also been used to study rainfall variability and extremes in Australia, with particular focus on the southeast of the country (Pook et al., 2006; Chubb et al., 2011; Risbey et al., 2013; Fiddes et al., 2015) and the eastern seaboard (Speer and Geerts, 1994; Callaghan and

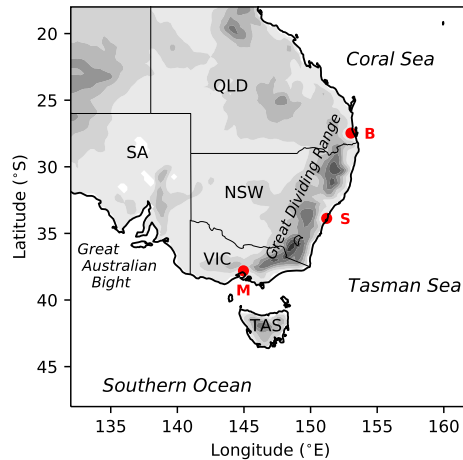


FIGURE 1 Map of southeast Australia showing surface topography (shading; 200 m intervals) and the locations of Brisbane (B), Sydney (S), and Melbourne (M). The states of Queensland (QLD), New South Wales (NSW), Victoria (VIC), South Australia (SA), and Tasmania (TAS) are also labelled together with key geographic features mentioned in the text.

48 Power, 2014). These studies again highlight the dominant contribution of frontal systems and cut-off lows to mean and extreme
 49 rainfall in southeast Australia, while coastal troughs, ECLs, and interactions with tropical systems drive precipitation extremes
 50 on the east coast.

51 The present study also uses a pattern-based approach to investigate extreme rainfall events in southeast Australia, but with
 52 a specific focus on distinguishing between more and less extreme cases. It is in part inspired by the work of Nuissier et al.
 53 (2011), which focussed on the LSCPs associated with precipitation extremes in southern France during the Boreal autumn
 54 (September–December). The authors defined two tiers of events, termed significant rainfall events (SREs) and heavy precipitation
 55 events (HPEs), based on, respectively, the 97 % and 99.9 % quantiles of daily precipitation for the period 1960–2000. They then
 56 used K-means clustering, applied to fields of 500 hPa geopotential height from the ERA-40 reanalysis (Uppala et al., 2005), to
 57 identify four LSCPs associated with these events. Composites of various quantities (e.g. quasi-geostrophic ascent, low-level
 58 moisture flux) were produced for each cluster and quantitatively compared between HPEs and non-HPEs (the subset of SREs
 59 not meeting the criteria for an HPE) to identify the key synoptic ingredients for the more extreme events. Following Plaut et al.
 60 (2001), the authors also used pattern correlations to assess the predictive power of the LSCPs for statistical downscaling of
 61 precipitation extremes.

62 Here we consider three domains centred on the major cities of Brisbane (state capital of Queensland, QLD), Sydney (state
 63 capital of New South Wales, NSW), and Melbourne (state capital of Victoria, VIC) (see Fig. 1 for locations). These are the
 64 three most populous cities in the country, with a combined population of over 12.5 million people (half the total population of
 65 Australia). For each domain, rain gauges are used to identify what we term *heavy rainfall events* (HREs) and *extreme rainfall*
 66 *events* (EREs), based on the 95th and 99th percentiles of wet-day (≥ 1 mm) rainfall, respectively. Following Nuissier et al.
 67 (2011), cluster analysis is then applied to reanalysis data from ERA5 (Hersbach et al., 2020) to identify the LSCPs associated
 68 with these events. Composite synoptic maps and vertical profiles are subsequently used to compare the large-scale and local
 69 environments of HREs and EREs. In addition, we examine the ability of both the identified circulation patterns and local
 70 column-integrated diagnostics to distinguish days with heavy or extreme rainfall.

The remainder of this paper is organised as follows. Section 2 describes the data and methods used to identify our events (2.1) and produce the LSCPs and associated composites (2.2). Section 3 then provides an overview of HRE and ERE characteristics, including their seasonal cycle and temporal association. Environmental characteristics of the events are then analysed in section 4, starting with an examination of the clusters, their relative frequency, and predictive power in identifying these rainfall events (4.1). This is followed by a detailed comparison of the synoptic patterns for HREs and EREs (4.2) and the characteristics of the atmospheric column in the vicinity of our three domains during these events (4.3). Finally, section 5 provides a summary of our results and recommendations for further work.

DATA AND METHODS

Rainfall data and event definitions

The rainfall events analysed in this study are defined based on daily rain gauge observations sourced from the Global Historical Climate Network-Daily (GHCN-D) database (Menne et al., 2012). Gauge data were selected over gridded precipitation products, such as the widely used Australian Water Availability Project dataset (Jones et al., 2009), to avoid the biases and uncertainties that are inevitably introduced in the gridding procedure (e.g. Tozer et al., 2012; King et al., 2013; Contractor et al., 2015). Note that, within Australia, daily rainfall observations cover the 24 h period up to 0900 local time, which for our three cities is either Australian Eastern Standard Time (AEST = UTC + 10 h) or Australian Eastern Daylight Time (AEDT = UTC + 11 h). Daylight Savings Time is observed from early October to early April in NSW and VIC. Although not currently observed in QLD, Daylight Savings Time was observed during the years 1989–1992.

Gauges within 75 km of the centre of Brisbane (153.03°E, 27.47°S), Sydney (151.21°E, 33.87°S), and Melbourne (144.96°E, 37.81°S) and with a record length of at least 30 years during the period 1979–2018 were first identified using the GHCN-D inventory. The 75 km threshold is somewhat arbitrary, but is large enough to encompass the urban areas of each city. Filtering was then applied to eliminate gauges with more than 30 % missing data during the study period as a whole or for any calendar month (following King et al., 2014), leaving a total of 79, 78, and 86 sites for the Brisbane, Sydney, and Melbourne domains, respectively. The spatial distribution of these gauges and their mean annual precipitation is shown in Fig. 2. On average precipitation is highest in Brisbane and lowest in Melbourne, but there is significant variability within each domain. Values range from 597 to 1654 mm in Brisbane, 616 to 1381 mm in Sydney, and 412 to 1370 mm in Melbourne.

To define events, we first identify wet days for each gauge, defined as those with at least 1 mm of accumulated daily rainfall. We then take the 95th and 99th percentiles of rainfall across these days as thresholds for heavy and extreme rainfall, respectively. These definitions are consistent with the indices R95pTOT (“rainfall on very wet days”) and R99pTOT (“rainfall on extremely wet days”) specified by the Expert Team on Climate Change Detection and Indices (Alexander et al., 2019). Since rainfall probability distributions vary between gauges, so do the heavy and extreme thresholds. Box-and-whisker plots of these thresholds for each domain are shown in Fig. 3. Median values for heavy rainfall in Brisbane, Sydney, and Melbourne are 45.6, 40.5, and 21.0 mm, respectively, while the corresponding values for extreme rainfall are 95.0, 81.0, and 38.4 mm. Note that for both thresholds, there is considerable overlap between the distributions for Brisbane and Sydney, but no overlap with the distribution for Melbourne.

In order for a day to be classified as an HRE or ERE, we require two gauges, separated by at least 50 km, to equal or exceed the corresponding percentile thresholds. This criterion is introduced to exclude localised events that are less likely to be associated with a pronounced synoptic-scale signature. A similar approach was used by Nuissier et al. (2011), albeit with a slightly higher distance threshold of 60 km. For the purpose of comparison with HREs and EREs, we also define rain events (REs) as days where two gauges, separated by at least 50 km, meet the wet-day threshold of 1 mm. Note that EREs represent a subset of HREs, which in turn represent a subset of REs. Table 1 summarises the event definitions and lists the number of events

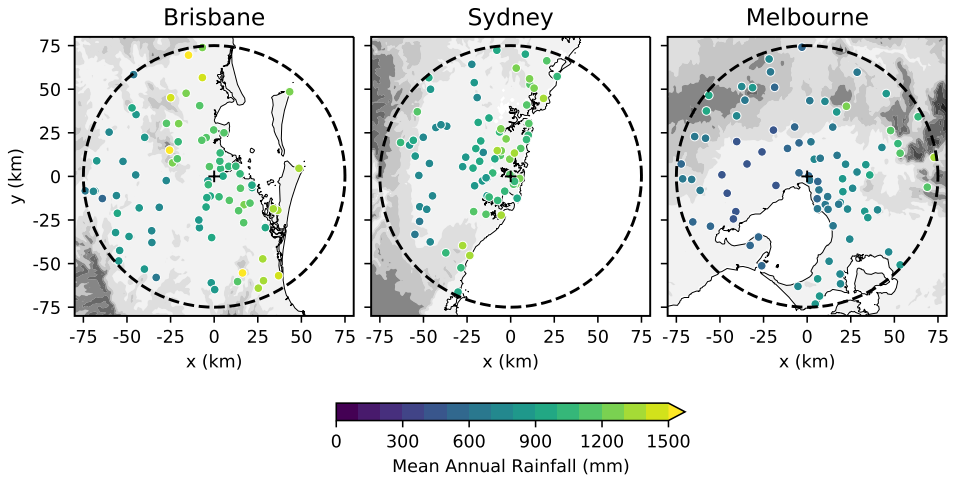


FIGURE 2 Maps showing surface topography (shading; 200 m intervals) and locations of rain gauges (filled circles, coloured according to mean annual rainfall in mm) for the (left to right) Brisbane, Sydney, and Melbourne domains. Crosses show the centre of each city and dashed lines mark a radius of 75 km.

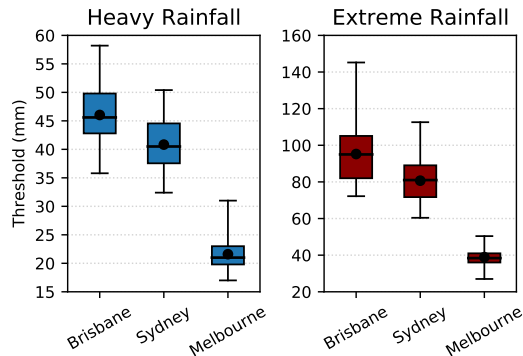


FIGURE 3 Box-and-whisker plots showing the distribution of thresholds for (left) heavy rainfall and (right) extreme rainfall across gauges in the three domains. Boxes show the interquartile range, whiskers show the minimum and maximum, horizontal bars show the median, and filled circles show the mean.

111 for each domain. On average there are approximately 192 REs, 16 HREs, and 3.5 EREs per year in Brisbane; 181 REs, 14 HREs,
 112 and 2.8 EREs per year in Sydney; and 213 REs, 22 HREs, and 5.9 EREs per year in Melbourne. The greater number of events in
 113 Melbourne likely reflects both a higher frequency of wet days (not shown) and the larger number of gauges. However, it may
 114 also be indicative of more widespread rainfall events in Melbourne and more localised events in Brisbane and Sydney. This can
 115 be seen if we express the number of events as a percentage of the number of days where a single gauge exceeds the relevant
 116 threshold (numbers in parentheses in Table 1). Values are somewhat higher for Melbourne, at least for REs and HREs, suggesting

TABLE 1 Definition of rainfall events considered in this study and number identified for each domain. Here, R95p and R99p indicate the 95th and 99th percentiles of wet-day (≥ 1 mm) rainfall, respectively. Values in parentheses express the number of events as a percentage of the number of days where only a single gauge exceeds the relevant rainfall threshold.

Event	Definition	Brisbane	Sydney	Melbourne
RE	Two gauges separated by at least 50 km with rainfall ≥ 1 mm	7678 (77.6)	7238 (72.6)	8504 (80.8)
HRE	Two gauges separated by at least 50 km with rainfall \geq R95p	635 (43.2)	571 (43.4)	867 (50.0)
ERE	Two gauges separated by at least 50 km with rainfall \geq R99p	138 (40.1)	111 (31.1)	237 (40.7)

117 that these events tend to be more widespread than in Brisbane and Sydney. For EREs, percentages are comparable for Brisbane
 118 and Melbourne but notably lower for Sydney, suggesting that extreme events are more localised in Sydney. For all three domains,
 119 the percentage decreases from REs to HREs to EREs, indicating the more localised nature of extreme rainfall in general.

120 | Reanalysis data and cluster analysis

121 Gridded data from the European Centre for Medium-range Weather Forecasts (ECMWF) fifth-generation reanalysis (ERA5;
 122 Hersbach et al., 2020) are used to characterise the environments of rainfall events considered in this study. ERA5 is the
 123 latest global reanalysis product released by ECMWF and replaces ERA-Interim (Dee et al., 2011), which ceased production
 124 in August 2019. Compared to ERA-Interim, it offers superior spatial and temporal resolution and incorporates a variety of
 125 newly reprocessed datasets and recent instruments that previously could not be assimilated. Our analysis makes use of hourly
 126 (near-)surface and pressure-level fields at 0.25° resolution on a square domain of 121×121 grid points covering $132\text{--}162^\circ\text{E}$ and
 127 $18\text{--}48^\circ\text{S}$ (Fig. 1).

128 Following previous studies in other parts of the world (e.g. Nuissier et al., 2011; Ohba et al., 2015; Grazzini et al., 2020), a set
 129 of representative large-scale circulation patterns (LSCPs) associated with HREs were defined using cluster analysis. Specifically,
 130 K-Means clustering was applied to daily-mean maps of mean sea-level pressure (MSLP) standardised anomalies. The anomalies
 131 are computed at every grid point as

$$\hat{p} = \frac{p - \bar{p}}{\sigma_p} \quad (1)$$

132 where p is the raw MSLP, \bar{p} and σ_p are, respectively, the 40-year mean and standard deviation for the corresponding calendar
 133 day, and \hat{p} is the standardised anomaly. MSLP is a useful field for characterising LSCPs outside of the tropics, as it represents
 134 variations in the mass of the atmospheric column (associated primarily with gradients in temperature) while also highlighting the
 135 near-surface circulation. Standardised anomalies were used in order to eliminate the seasonal cycle, which would otherwise
 136 dominate the clusters. The daily mean was used in the absence of any information regarding the sub-daily evolution of events. To
 137 simplify data processing, the daily mean was computed using hourly fields for 0000–2300 UTC the day prior to the nominal
 138 event date. There is thus a 1–2 h offset (2 h during daylight savings; 1 h the rest of the year) between the period during which
 139 rainfall was recorded and the period used in the synoptic analysis.

140 Clustering was performed using the *scikit-learn* module for Python (Pedregosa et al. 2011), with *k-means++* initialisation and
 141 a fixed random state to make the results deterministic (see <https://scikit-learn.org/stable/modules/generated/sklearn.cluster.KMeans.html>). Following some experimentation, the number of clusters was set to three as a compromise
 142 between minimising within-cluster variance while maintaining interpretability. Inevitably, some samples are poorly represented
 143 by the set of clusters. To deal with these, we apply filtering following a method similar to that proposed by Huva et al. (2014)
 144 for self-organizing maps. Specifically, we compute the absolute difference in \hat{p} between each sample and its nearest cluster
 145

centroid, denoted $\Delta\hat{\rho}$, for every grid point in the domain. We then identify those samples where the average $\Delta\hat{\rho}$ over the domain $\Delta\hat{\rho}_{\text{avg}} > 1$ and/or the maximum $\Delta\hat{\rho}$ over the domain $\Delta\hat{\rho}_{\text{max}} > 3$ and assigned these to a separate “rejected” category. These thresholds were selected to cut off the long tail of the $\Delta\hat{\rho}_{\text{avg}}$ and $\Delta\hat{\rho}_{\text{max}}$ distributions (not shown). A total of 45 (7.1 %), 29 (5.1 %), and 62 (7.2 %) samples are rejected for the Brisbane, Sydney, and Melbourne domains, respectively. Note that while $\Delta\hat{\rho}_{\text{avg}}$ and $\Delta\hat{\rho}_{\text{max}}$ are correlated ($r \approx 0.6$), both thresholds contribute to the rejection of samples.

1 HEAVY AND EXTREME RAINFALL EVENT CHARACTERISTICS

Figure 4 shows box-and-whisker plots of the frequency of REs, HREs, and EREs across all gauges in each domain, along with the percentage contribution of these events to total rainfall at each gauge. As previously noted, all three classes of event occur more frequently in Melbourne than in Brisbane and Sydney; however, they represent a significantly smaller contribution to total rainfall. This reflects the more common occurrence of light precipitation in the oceanic midlatitude climate of Melbourne compared to the subtropical environments of Sydney and Brisbane. While heavy and extreme events occur infrequently, they represent a significant contribution to total rainfall. HREs occur on $\sim 1\%$ of days yet typically account for $>20\%$ of total rainfall in Melbourne and $>25\%$ in Brisbane and Sydney. These results are consistent with Pendergrass and Knutti (2018), who found that the 95th percentile of wet-day rainfall contributes 24 % of annual rainfall when considering the median across GHCN-D stations globally (their Table 1). Meanwhile, EREs occur on $\sim 0.2\%$ of days but, for the majority of gauges, represent at least 6 % of total rainfall in Melbourne and at least 8 % in Brisbane and Sydney. Note that qualitatively similar results are obtained if we consider wet days, and days with heavy and extreme rainfall at individual gauges (i.e. without the event criterion of two gauges separated by at least 50 km), but with slightly higher percentages.

Figure 5 shows the seasonal cycle of REs, HREs, and EREs in each domain. For REs, Brisbane and Sydney show a similar distribution, with fairly uniformly high frequencies of $\sim 10\%$ during the extended summer season (November to March) and a minimum in August. The seasonal cycle for HREs in those two cities is broadly similar, but with a higher amplitude. The maximum frequency occurs in December for Brisbane but not until March for Sydney. Both domains show low HRE frequency during late winter, with a minimum in September for Brisbane and July for Sydney. Due to a smaller sample size (Table 1), the distributions for EREs are quite noisy (particularly for Sydney) but suggest an even more amplified seasonal cycle. The month of February accounts for almost 20 % of events in Sydney and 25 % of events in Brisbane. No EREs are identified during the months of August and September in Brisbane and only two occur in July. On the other hand, Sydney shows higher relative frequencies for EREs compared to HREs during the winter months, particularly in August. This may reflect the climatology of ECLs, which occur most frequently in late winter to early spring (Pepler et al., 2015; Cavicchia et al., 2019) and often give rise to extreme rainfall in this region (Callaghan and Power, 2014; Pepler et al., 2014). The seasonal cycle of events in Melbourne is notably different. REs show a pronounced winter peak, with frequencies above 10 % in July and August, and a minimum in February. In contrast, the distribution for HREs is quite flat across the year, with only slightly higher frequencies in spring and early summer. The seasonal cycle of EREs is again noisier, but shows a clear summer peak, with over 50 % of events occurring from November to February (and nearly 30 % in November and December alone), while the minimum is in August.

To illustrate the temporal association between events, Fig. 6 shows the probability of an HRE as a function of the day relative to both HREs and EREs for lags ranging from one week before the event to one week after the event. To assess whether these probabilities are significantly different from the HRE base rate we use the binomial distribution. For a given lag, the probability that the number of events N exceeds some threshold x is given by

$$\Pr \{N \geq x\} = \sum_{k=x}^N \frac{N!}{k! (N-k)!} P^k (1-P)^{N-k} \quad (2)$$

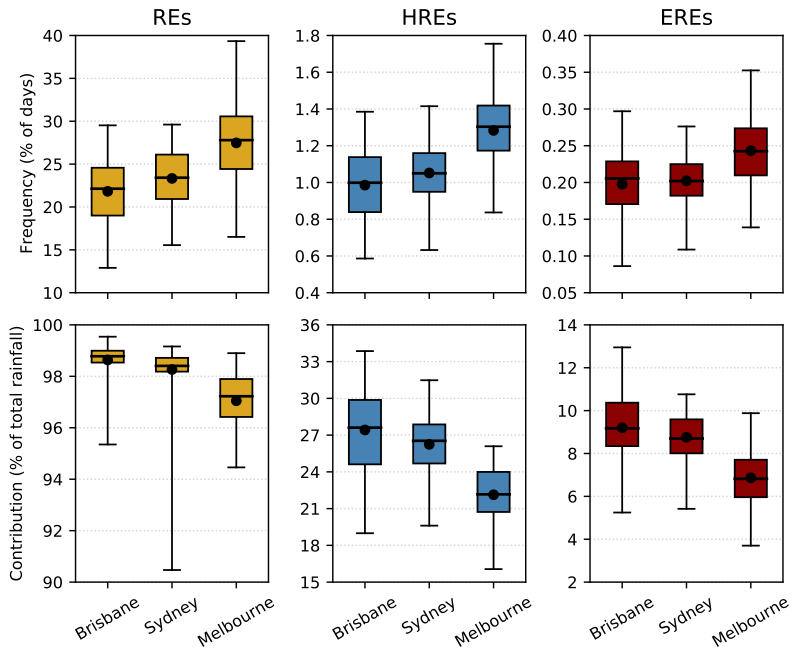


FIGURE 4 Box-and-whisker plots showing the (top) frequency and (bottom) contribution to total rainfall of (left to right) REs, HREs, and EREs across gauges in the three domains. Boxes show the interquartile range, whiskers show the minimum and maximum, horizontal bars show the median, and filled circles show the mean.

183 where $P = N_{\text{HRE}}/N_{\text{TOT}}$ is the base rate probability for HREs, N_{HRE} is the number of HREs, and N_{TOT} is the total number of
 184 days in the analysis. Differences are said to be statistically significant when $\text{Pr} < 0.01$ (indicating probabilities much larger than
 185 the base rate) or when $\text{Pr} > 0.99$ (indicating probabilities much smaller than the base rate).

186 Figure 6 shows that the probability of an HRE is elevated on days immediately leading up to and following an event,
 187 indicating that events often span multiple days. For HREs, the difference is significant out to ± 5 days for Brisbane, ± 4 days for
 188 Sydney, and ± 2 days for Melbourne. The more rapid drop off in probabilities either side of events in Melbourne likely reflects the
 189 more transient nature of the synoptic systems that bring intense precipitation to this region (see section 4.2). In all three domains,
 190 probabilities are higher for EREs than HREs, indicating that extreme events are more likely to be embedded in a multi-day HRE.
 191 Overall, the fraction of HREs (EREs) that occur as part of a multi-day HRE is 30.6 % (56.5 %) for Brisbane, 35.0 % (55.9 %) for
 192 Sydney, and 23.2 % (34.1 %) for Melbourne. As we might expect, multi-day EREs are rarer, but still account for around a fifth of
 193 these events in each city (23.9 % in Brisbane, 22.5 % in Sydney, and 19.4 % in Melbourne).

194 | ENVIRONMENTS OF HEAVY AND EXTREME RAINFALL EVENTS

195 | Categorising synoptic environments

196 As detailed in section 2.2, the synoptic environments associated with heavy and extreme rainfall in each domain were categorised
 197 by applying K-means clustering to maps of the daily mean standardised MSLP anomaly, \hat{p} . The corresponding maps for each

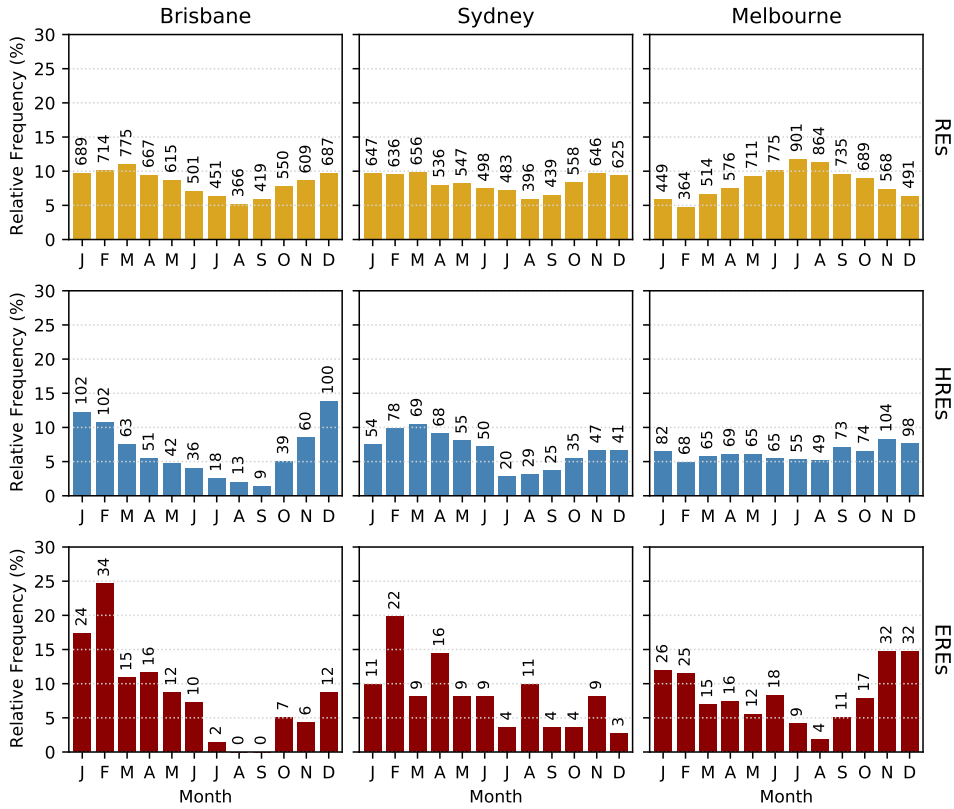


FIGURE 5 Histograms showing the relative frequency of (top to bottom) REs, HREs, and EREs as a function of the month of the year in the (left to right) Brisbane, Sydney, and Melbourne domains. Numbers above the bars show the event count for each month.

198 cluster centroid are shown in Fig. 7. Note that the clusters for each domain were numbered so that domain-mean $\hat{\rho}$ increases from
 199 Cluster 1 to Cluster 3. Two of the three Brisbane clusters (Clusters 2 and 3) and all three of the Sydney clusters are characterised
 200 by a north-to-south gradient in $\hat{\rho}$, implying easterly geostrophic wind anomalies. While the position and relative amplitude of the
 201 associated high- and low-pressure anomalies varies between clusters, this basic pattern is consistent. Cluster 1 for Brisbane is
 202 slightly different, showing a dominant negative MSLP anomaly centred over southeast Queensland, implying more of a northerly
 203 geostrophic wind anomaly in Brisbane. For Melbourne, all three clusters feature negative $\hat{\rho}$ over the city. Clusters 1 and 2 show
 204 a strong negative pressure anomaly to the northwest and east of Melbourne, respectively, while Cluster 3 features a weaker
 205 negative anomaly centred directly over the city. Further analysis of the synoptic patterns associated with each cluster is presented
 206 in section 4.2.

207 HREs and EREs were assigned to the clusters based on Euclidean distance, with a minority of events rejected from the
 208 clusters due to large differences in domain-mean or maximum $\hat{\rho}$ (section 2.2). Table 2 lists the number and percentage of HREs
 209 and EREs assigned to each cluster or rejected from the clusters. For all three domains, Cluster 3 makes up the largest percentage
 210 of HREs, while for Brisbane and Sydney, Cluster 1 represents a notably smaller percentage. These results may in part reflect the

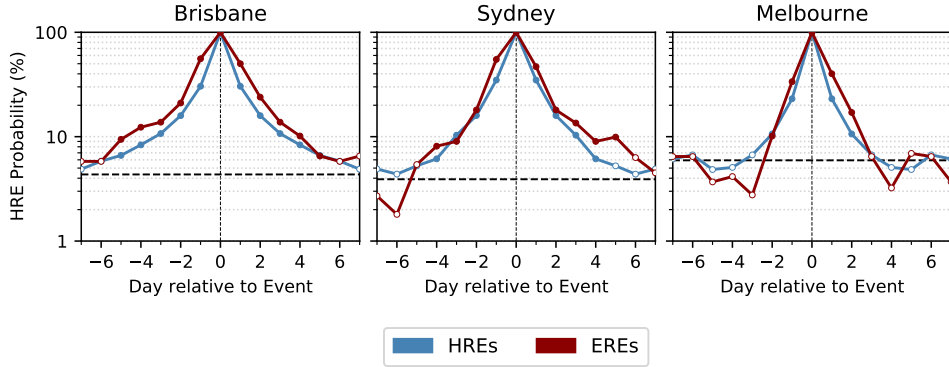


FIGURE 6 Probability of an HRE as a function of the day relative to HREs and EREs in the (left to right) Brisbane, Sydney, and Melbourne domains. Filled markers indicate probabilities that are statistically significantly different from the climatological value (indicated by the dashed horizontal lines).

TABLE 2 Number and percentage (in parentheses) of HREs and EREs assigned to the three clusters or rejected from the clusters in each domain.

Domain	Event	Cluster 1	Cluster 2	Cluster 3	Rejected
Brisbane	HRE	123 (19.4)	219 (34.5)	248 (39.1)	45 (7.1)
	ERE	22 (15.9)	75 (54.3)	25 (18.1)	16 (11.6)
Sydney	HRE	128 (22.4)	185 (32.4)	229 (40.1)	29 (5.1)
	ERE	26 (23.4)	40 (36.0)	37 (33.3)	8 (7.2)
Melbourne	HRE	253 (29.2)	234 (27.0)	318 (36.7)	62 (7.2)
	ERE	66 (30.4)	46 (21.2)	87 (40.1)	18 (8.3)

211 fact that large-amplitude pressure anomalies occur less frequently than lower amplitude anomalies (Cluster 3 has the smallest
 212 anomalies for all three domains, while Cluster 1 has the largest anomalies for Brisbane and Sydney). For EREs, the split between
 213 the three clusters changes only slightly for Sydney and Melbourne: a higher proportion of events are associated with Cluster 2
 214 in Sydney and with Cluster 3 in Melbourne. For Brisbane we see a more dramatic change, with over half of EREs associated
 215 with Cluster 2 and a much smaller proportion associated with Cluster 3. This is consistent with the stronger north-to-south
 216 pressure gradient for Cluster 2, which, as we will show, promotes stronger onshore flow and associated moisture anomalies. The
 217 proportion of rejected events is also larger for EREs, particularly for Brisbane, indicating that extreme events are more likely to
 218 be associated with LSCPs that differ significantly from the cluster centroids shown in Fig. 7. Note that we do not find clear
 219 seasonal cycles in the proportion of HREs and EREs assigned to each cluster (not shown). This is perhaps to be expected given
 220 our use of standardised MSLP anomalies, which eliminates seasonal variations in anomaly magnitude.

221 The clusters shown in Fig. 7 broadly represent the spectrum of LSCPs associated with HREs in the three domains. However,
 222 one might ask how often similar patterns occur on days that don't produce an HRE. A related question is: to what extent do
 223 these patterns represent a sufficient condition for heavy or extreme precipitation in each domain? To address these questions, we
 224 compute the pattern correlation r between each cluster centroid and the map of standardised pressure anomaly for every day in

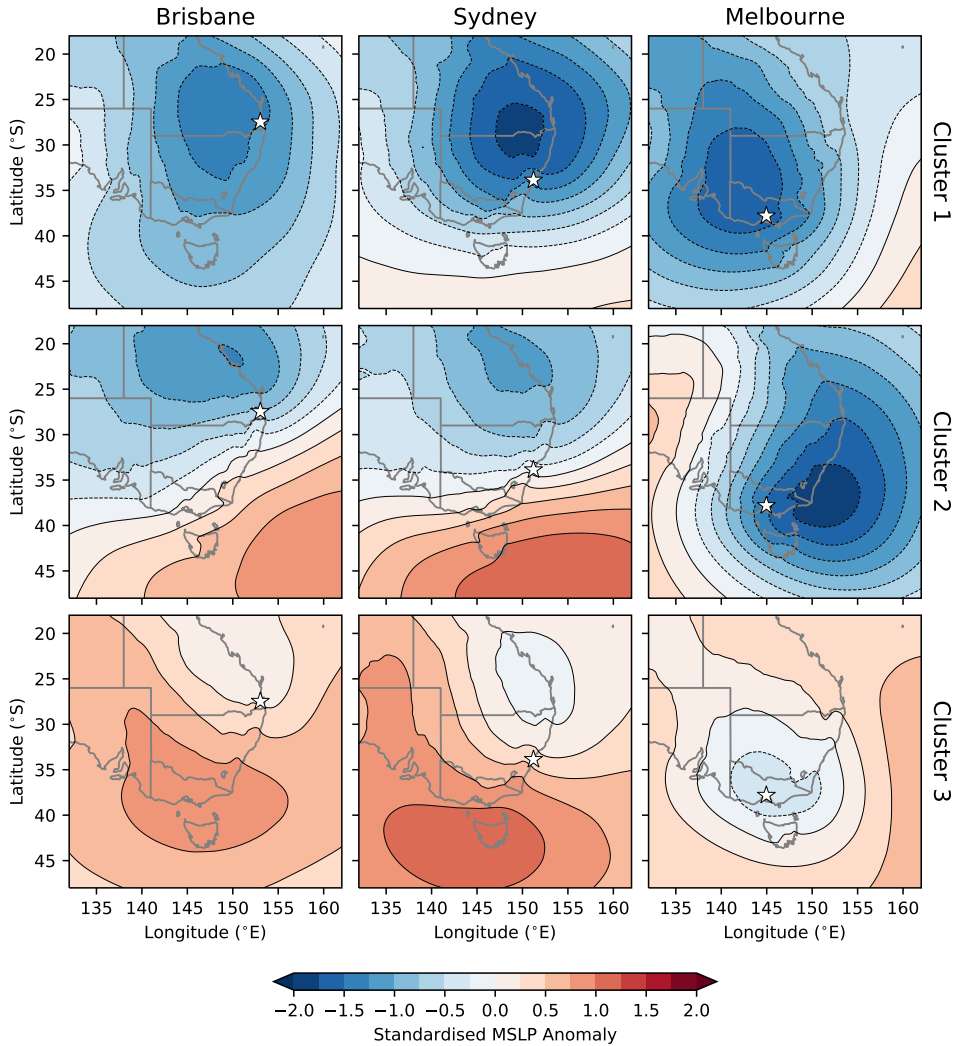


FIGURE 7 Standardised anomalies of MSLP (unitless) corresponding to the centroids of the three clusters for (left to right) Brisbane, Sydney, and Melbourne. Stars show the locations of the cities.

225 the 40-year study period. Days are then binned according to their pattern correlation and the relative frequency is computed
 226 together with the probability of HREs and EREs for each bin. We also compute the probability of REs for each bin in order
 227 to explore the relationship between the clusters and rainfall more generally. To assess whether probabilities are significantly
 228 different from the base rate for each event type we again make use of the binomial distribution (Eq. 2). Figure 8 shows the results
 229 of this analysis.

230 For all three domains we see that strong positive pattern correlations ($r > 0.6$) are relatively rare (especially for Clusters 1
 231 and 3 in Brisbane and Cluster 3 in Melbourne), but are associated with a significantly elevated probability of heavy and extreme

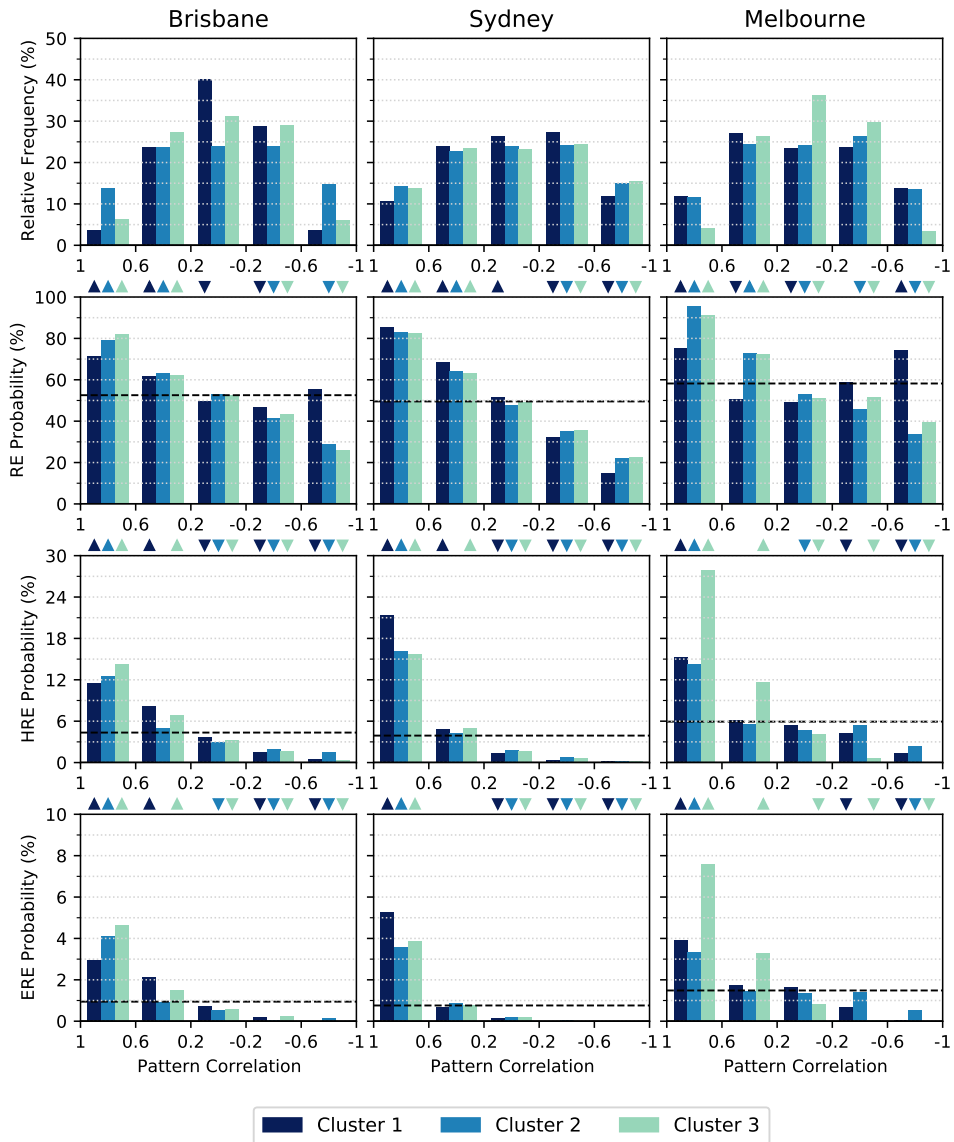


FIGURE 8 Bar charts showing (top to bottom) the relative frequency of days with different pattern correlations and the probability of REs, HREs, and EREs as a function of pattern correlation for each of the three clusters in the (left to right) Brisbane, Sydney, and Melbourne domains. Upward and downward triangles indicate where the event probability is significantly higher and lower, respectively, than the climatological event probability (dashed line).

232 rainfall. This is particularly true for Cluster 3 in Melbourne, which shows HRE and ERE probabilities that are around five
 233 times the base rate (this increases to around 10 times the base rate for $r > 0.8$; not shown). Conversely, strong negative
 234 correlations ($r < -0.6$) are associated with a significantly diminished probability of HREs and EREs. These results demonstrate

a robust association between the identified LSCPs and the occurrence of heavy and extreme rainfall in all three domains. For most clusters, this association extends to rainfall more generally, with a monotonic increase in the probability of REs for increasing pattern correlation. The relationship is more ambiguous for Cluster 1 in Brisbane and Cluster 1 in Melbourne, with the latter showing significantly enhanced RE probabilities for both strong positive and strong negative correlations. On the other hand, Clusters 2 and 3 in Brisbane and all three Sydney clusters show a clear transition from significantly elevated RE probabilities for positive r to significantly diminished RE probabilities for negative r . This result is consistent with Black and Lane (2015), who found a strong relationship between the meridional pressure gradient and summertime rainfall along the east coast of Australia.

Synoptic circulation and moisture characteristics

In this section, we use composite maps to more fully characterise the synoptic circulations associated with HREs and EREs in each domain. Separate maps are produced for each cluster by averaging over the days assigned to that cluster and then smoothing the resulting fields using a Gaussian kernel with a standard deviation of two grid points (0.5°) and a radius of three standard deviations (1.5°). Consistent with the cluster analysis (section 2.2), daily-mean (00–23 UTC) fields were used for each event. Smoothing was applied simply to reduce noise, which remains pronounced for some fields due to the relatively high resolution of ERA5. Figures 9 and 10 show composite maps for HREs and EREs assigned to each of the Brisbane clusters. Figure 9 shows the 500 hPa geopotential height, MSLP, and 10 m winds, to capture the near-surface and midlevel circulations, while Fig. 10 shows column water vapour (CWV), 500 hPa pressure vertical velocity ω , and integrated vapour transport (IVT; defined as the column integral of the product of horizontal mass flux and specific humidity), to illustrate differences in moisture and large-scale ascent. Equivalent maps for Sydney are shown in Fig. 11 and 12 and for Melbourne in Fig. 13 and 14. Note that the comparison between HREs and EREs in this section is largely qualitative in nature. A quantitative comparison of selected parameters at the location of each city is provided in section 4.3.

Focussing first on HREs in Brisbane (Fig. 9 and 10, top row), we see that Cluster 1 is characterised by an MSLP trough over inland eastern Australia, with high pressure to the west and east (centred in the Great Australian Bight and over the Tasman Sea, respectively), while Clusters 2 and 3 feature a more zonally elongated high-pressure system that stretches west from the Tasman Sea across Victoria and Tasmania. The centre of this high is located farther to the east for Cluster 2, with a stronger meridional pressure gradient compared to Cluster 3. Clusters 2 and 3 also feature ridging along the east coast of the continent associated with the Great Dividing Range. Surface winds around Brisbane are directed onshore, from the north-northeast in Cluster 1, the east-northeast in Cluster 2, and the east in Cluster 3. At 500 hPa, all three clusters feature a trough to the west of Brisbane; however, the orientation of this feature varies, with a pronounced negative tilt for Cluster 2, a slight positive tilt for Cluster 3, and minimal tilt for Cluster 1. Positive CWV anomalies (exceeding 10 mm) and ascent ($\omega < -5$ hPa/h) are centred over Brisbane in each case, with northwesterly IVT for Cluster 1 and northeasterly IVT for Clusters 2 and 3. The overall patterns for EREs (Fig. 9 and 10, bottom row) are broadly similar, but characterised by a more amplified midlevel trough, stronger MSLP gradients and surface winds, larger CWV anomalies and IVT, and stronger vertical motion. For Cluster 1, we also observe a change in the orientation of the IVT vectors around Brisbane, from northwesterly for HREs to more northerly for EREs.

For Sydney (Fig. 11 and 12), all three clusters show a north-to-south pressure gradient with easterly to southeasterly onshore flow along the NSW coast. The MSLP pattern for Cluster 1 is characteristic of an east coast low (ECL) (e.g. Holland et al., 1987; Speer et al., 2009; Dowdy et al., 2019), with a closed low just offshore of northern NSW cradled by a ridge to the south of the continent. In place of a closed low, Clusters 2 and 3 feature a coastal trough (interrupted by ridging along the Great Dividing Range), with a strong, zonally elongated high-pressure system centred to the east (Cluster 2) or west (Cluster 3) of Tasmania. Similar to Brisbane, all three clusters feature a 500 hPa trough to the west of the region of interest, with positive CWV anomalies and large-scale ascent centred over Sydney. Comparing EREs and HREs, we again see a more amplified upper trough (with a cut-off low for Cluster 2), stronger meridional pressure gradients and onshore flow at the surface, larger CWV anomalies and

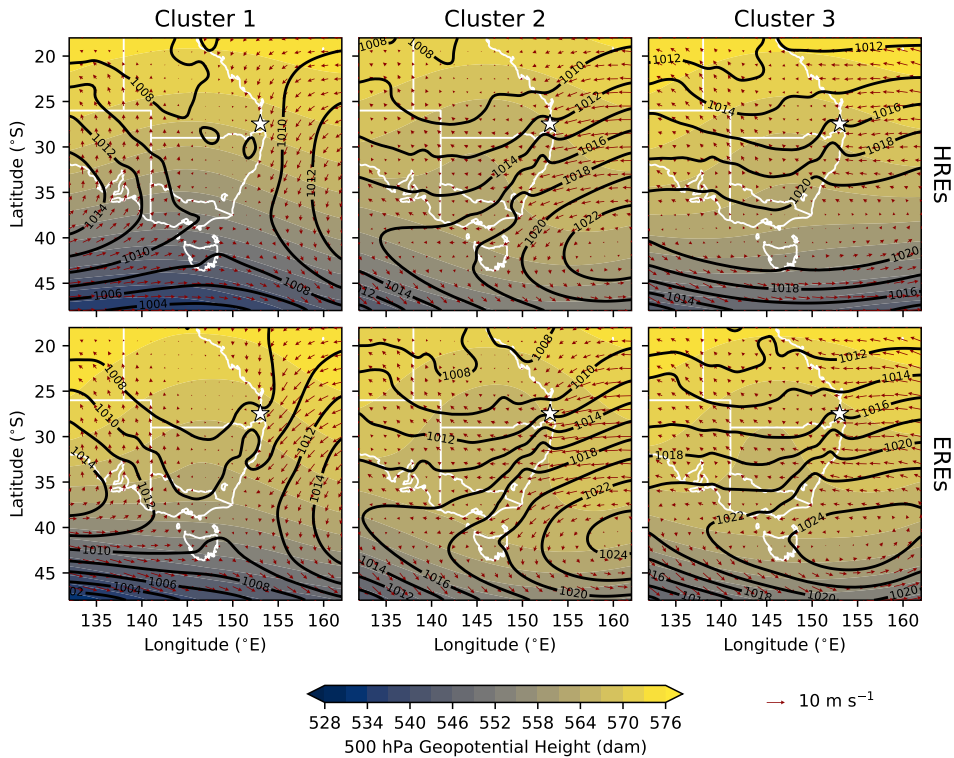


FIGURE 9 Composite maps of 500 hPa geopotential height (shading; dam), MSLP (thick contours; hPa), and 10 m winds (vectors) for (top) HREs and (bottom) EREs for each of the Brisbane clusters. All fields have been smoothed using a Gaussian kernel with a standard deviation of two grid points (0.5°).

276 IVT, and stronger midlevel ascent associated with the extreme events.

277 Before discussing the synoptic composites for Melbourne, it is worth providing a brief comparison of our results for Sydney
 278 and Brisbane with those of Callaghan and Power (2014). They analysed weather patterns associated with major floods along a
 279 portion of the east coast (extending from the VIC–NSW border to Brisbane) during the period 1860–2012. All events were found
 280 to be associated with an ECL (either a closed low or coastal trough) or what the authors termed “tropical interactions” (TIs). The
 281 latter were subdivided into three types, characterised by (1) a tropical cyclone, (2) a midlatitude trough interacting with a tropical
 282 cyclone/low or inland trough, and (3) a transitioning tropical cyclone/low. For the period during which our two studies overlap
 283 (1979–2012) there were 61 flood events, 56 of which coincided with an HRE in Brisbane and/or Sydney. The vast majority of
 284 these ($47/56 = 83.9\%$) were EREs. Of the overlapping events, 33 (58.9%) were classified by Callaghan and Power as ECLs, 10
 285 (17.9%) were classified as Type 2 TIs, and 13 (23.2%) were classified as Type 3 TIs (the handful of Type 1 TIs all occurred
 286 prior to 1979). We did not find a clear association between our clusters and the weather patterns defined by Callaghan and Power.
 287 However, we note that none of our composites for Brisbane and Sydney feature a tropical cyclone/low signature. Furthermore, of
 288 the 13 overlapping events classified as Type 3 TIs by Callaghan and Power, four were rejected from our clusters. This suggests
 289 that tropical systems may be underrepresented in our analysis, due to the small-scale, high-amplitude nature of their associated
 290 pressure anomalies, which are poorly captured by the clusters.

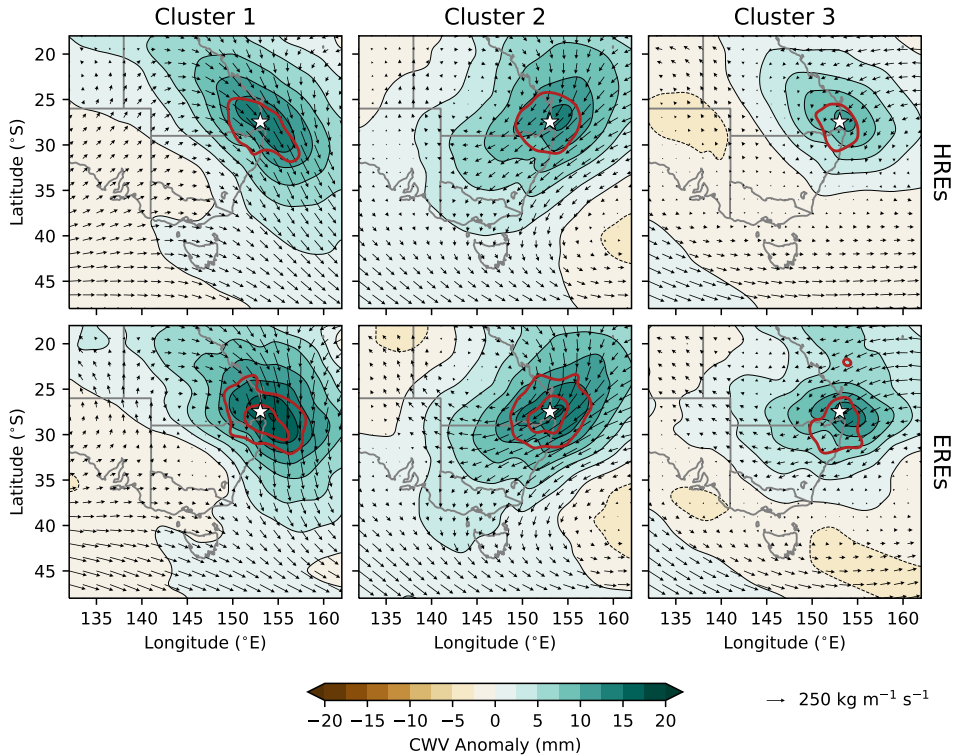


FIGURE 10 Composite maps of column water vapour (CWV) anomalies (shading; mm), 500 hPa pressure vertical velocity (thick contours at -5 and -10 hPa/h), and integrated vapour transport (vectors) for (top) HRES and (bottom) ERES for each of the Brisbane clusters. All fields have been smoothed using a Gaussian kernel with a standard deviation of two grid points (0.5°).

291 Compared to Brisbane and Sydney, the Melbourne clusters show more distinct synoptic patterns (Fig. 13 and 14). Cluster 1
 292 is characterised by a high-amplitude MSLP trough, indicative of a surface cold front, to the west of the city, with a high in the
 293 Tasman Sea and north to northeasterly flow at the surface. Strong northwesterly IVT, accompanied by positive CWV anomalies
 294 and midlevel ascent are present over Melbourne, consistent with the presence of a warm conveyor belt (e.g. Browning 1986)
 295 ahead of the approaching front. Cluster 2 meanwhile features a closed low to the east of Tasmania, with south to southwesterly
 296 flow over Victoria. CWV anomalies are notably lower for this cluster, consistent with the southwesterly IVT (directed from the
 297 cool Southern Ocean) and strong midlevel ascent is absent over Melbourne. Clusters 1 and 2 both feature a deep 500 hPa trough
 298 to the west of the surface trough/low, with strong geopotential height gradients indicating the presence of an upper-level jet
 299 streak. In contrast, Cluster 3 suggests more quiescent conditions, with an inland trough extending south from central Queensland,
 300 weak pressure gradients over much of eastern Australia, and a lower-amplitude 500 hPa trough to the west of Melbourne. Similar
 301 to Cluster 1, this cluster features northwesterly IVT and midlevel ascent over Melbourne; however, both are weaker. Comparing
 302 ERES and HRES we observe little difference in the MSLP patterns for Clusters 1 and 3, but a more amplified midlevel trough,
 303 favouring stronger ascent over Melbourne. CWV anomalies are also enhanced, consistent with the results for Brisbane and
 304 Sydney. For Cluster 2, the surface low is displaced to the northwest for ERES, resulting in a stronger pressure gradient and
 305 more southerly flow over Melbourne. At 500 hPa there is a cut-off low, with the associated circulation promoting ascent and the

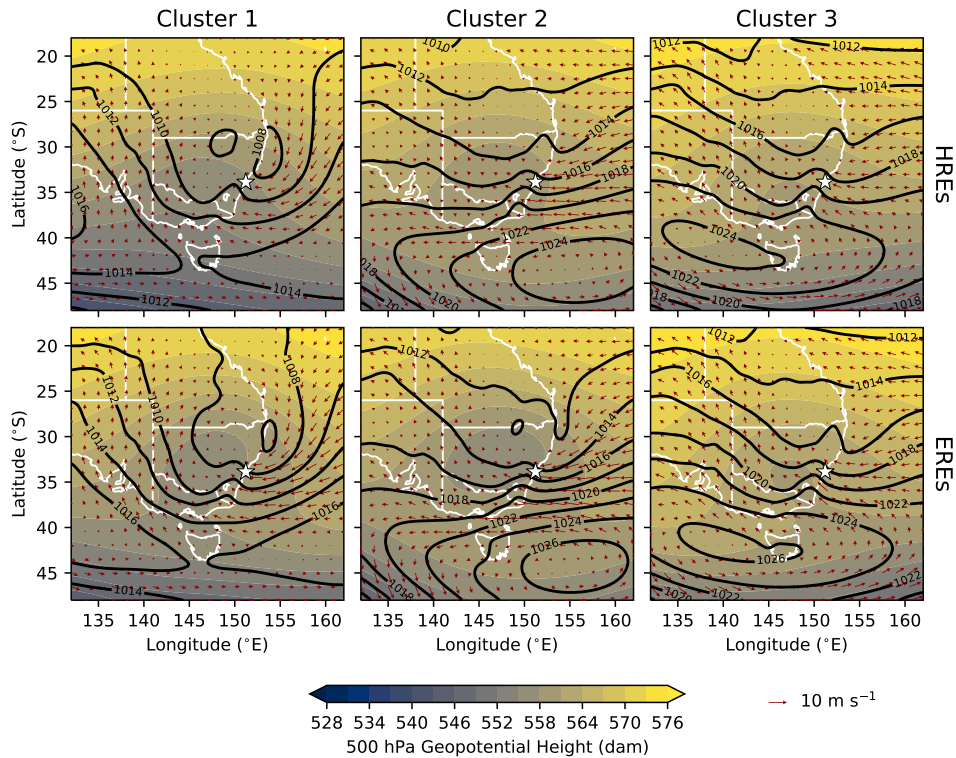


FIGURE 11 As in Fig. 9 but for each of the Sydney clusters.

transport of larger CWV into Victoria from the Tasman Sea.

While it is not possible to unambiguously quantify the location of moisture sources from the present analysis, the northward extension of strong IVT and positive CWV anomalies (Fig. 10, 12, and 14) suggest that tropical moisture is being transported into the study regions during heavy and extreme rainfall events. For Brisbane and Sydney, this moisture appears to originate over the Coral Sea, consistent with the back-trajectory analysis of Holgate et al. (2020) (their Supplementary Fig. 11). As noted above, the ERE composite for Cluster 2 in Melbourne suggests transport of moisture from the Tasman Sea around the surface low pressure system. The pattern of CWV anomalies and IVT for Cluster 1 (and, to a less degree, Cluster 3) in Melbourne suggests that moisture is being sourced from the tropical east Indian Ocean. However, Holgate et al. (2020) found no evidence that precipitation in southeast Australia relies on moisture from the northwest. Instead, they showed that most moisture in this region is sourced from the Tasman Sea (their Supplementary Fig. 11). On the other hand, Hauser et al. (2020) identified a distinct northwest pathway for moisture transport associated with warm conveyor belt rainfall in southeast Australia. Given this inconsistency, and the fact that both studies focussed primarily on monthly mean rainfall, we suggest that further work is needed to understand the moisture sources for short-duration Australian rainfall extremes.

As noted in the introduction, the analysis presented in this and the previous section was to a large degree inspired by the work of Nuissier et al. (2011). They used K-Means clustering to identify four LSCPs associated with “significant rain events” in southern France during the Boreal autumn. Consistent with our results for Brisbane, Sydney, and Melbourne, all four of these patterns featured an upper-level trough either upstream of or directly over the study region. For the three dominant clusters

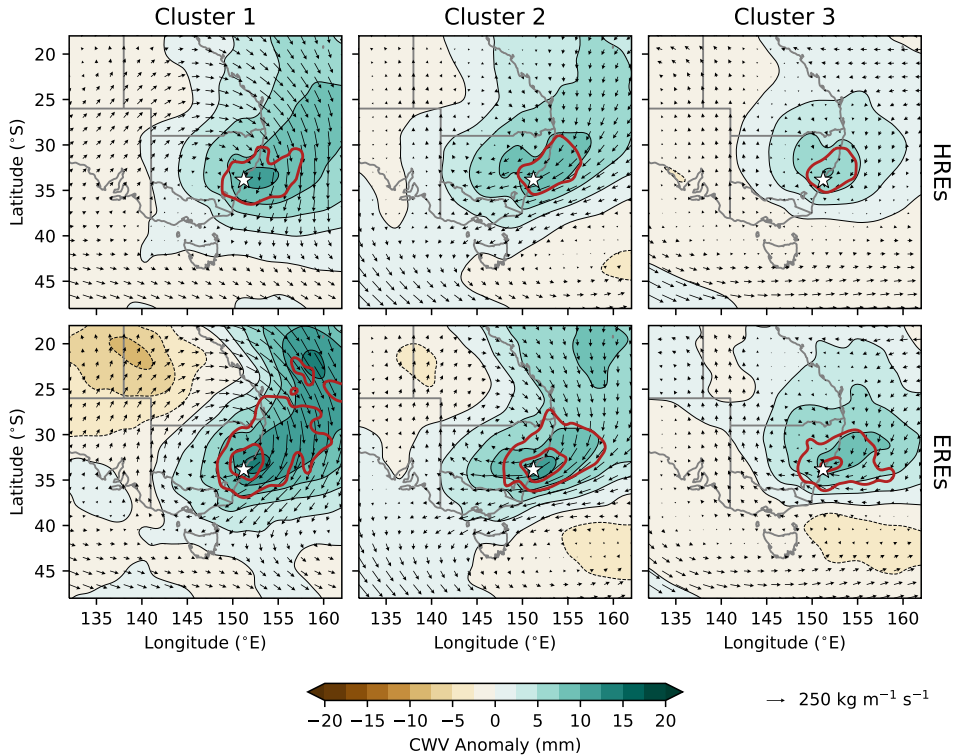


FIGURE 12 As in Fig. 10 but for each of the Sydney clusters.

323 (which collectively accounted for nearly 85 % of events), synoptic composites were produced for more and less extreme subsets
 324 of the events, termed HPEs (heavy precipitation events) and non-HPEs, respectively. These revealed the presence of moist
 325 onshore (south to southeasterly) low-level winds and synoptically forced ascent over the study region, with larger moisture fluxes
 326 and stronger ascent for the HPE composites (c.f. Fig. 10, 12, and 14), associated with a more amplified upper-level pattern
 327 (c.f. Fig. 9, 11, and 13). Thus, despite distinct geographical settings, there appear to be many similarities between the LSCPs
 328 associated with heavy and extreme rainfall events in southern France and southeast Australia.

329 | Local thermodynamic and circulation characteristics

330 Complementing the synoptic analysis presented above, this section explores the characteristics of the environment in the
 331 immediate vicinity of HREs and EREs in each domain using vertical profiles and a selection of column-integrated diagnostics.
 332 Figure 15 shows composite Skew- T -log- p diagrams for the HREs and EREs assigned to each cluster in Brisbane, Sydney,
 333 and Melbourne. To produce these plots, daily-mean (00–23 UTC) fields of temperature, dewpoint temperature (derived from
 334 temperature and relative humidity), and zonal and meridional wind on pressure levels were extracted for 3×3 grid columns
 335 (i.e. a $0.75^\circ \times 0.75^\circ$ area) centred on the grid point closest to each city and horizontally averaged. Surface-level fields (surface
 336 pressure, 2 m temperature and dewpoint temperature, and 10 m winds) for the same area were similarly extracted and averaged
 337 before being inserted into the columns at the appropriate level (disregarding data on pressure levels below the surface). The

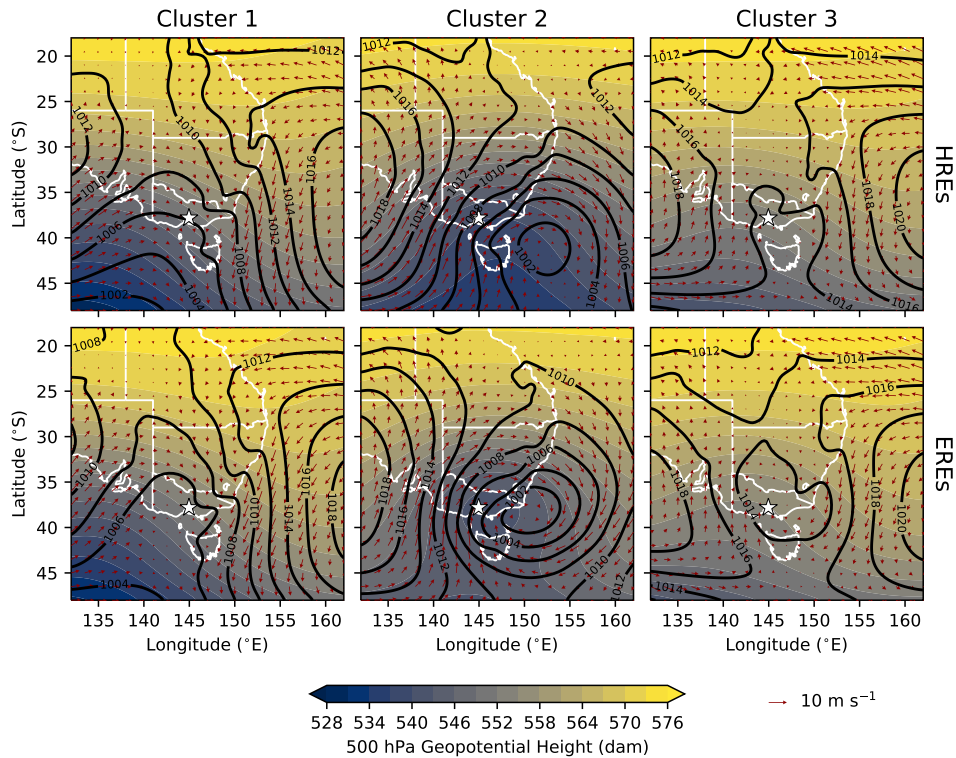


FIGURE 13 As in Fig. 9 but for each of the Melbourne clusters.

338 profiles were then linearly interpolated to a regular height grid, extending from the surface to 20 km above ground level (AGL)
 339 with 100 m grid spacing, before finally being composited for the various event subsets. Using height AGL rather than pressure as
 340 the vertical coordinate simplifies the averaging of profiles with different surface pressures, while horizontal averaging over 3×3
 341 grid points smooths data to a resolution more consistent with the scale of our events (i.e. at least 50 km).

342 Figure 15 shows that all of the profiles are characterised by high moisture content throughout the troposphere, with lapse
 343 rates close to moist-neutral and small dewpoint depressions, particularly below 700 hPa. For Brisbane and Sydney, the wind
 344 profiles show strong anticyclonic turning with height below 500 hPa, with southeasterly to northeasterly surface winds and
 345 westerly or northwesterly flow at upper levels. This finding is consistent with Callaghan and Power (2016), who identified a very
 346 similar wind structure associated with major flooding events along the east coast of Australia. For Melbourne, wind profiles are
 347 more unidirectional (although Cluster 1 shows some anticyclonic turning in the lowest few kilometres), with predominantly
 348 northwesterly flow for Clusters 1 and 3 and west-southwesterly flow for Cluster 2.

349 Comparing HREs and EREs, we see that free tropospheric dewpoints are typically higher for the latter, consistent with
 350 the higher CWV anomalies seen in the composite synoptic maps (Fig. 10, 12, and 14). In Melbourne, extreme events are also
 351 characterised by a warmer column, particularly for Clusters 1 and 2. This is in line with the finding that EREs occur most
 352 frequently during the summer months, while HREs are more evenly distributed across the year (Fig. 5). For Brisbane and
 353 Sydney, the most striking difference between EREs and HREs is the presence of stronger and deeper easterly flow in the lower
 354 troposphere for the extreme events. In general, winds with an easterly component extend at least 1 km higher and have maximum

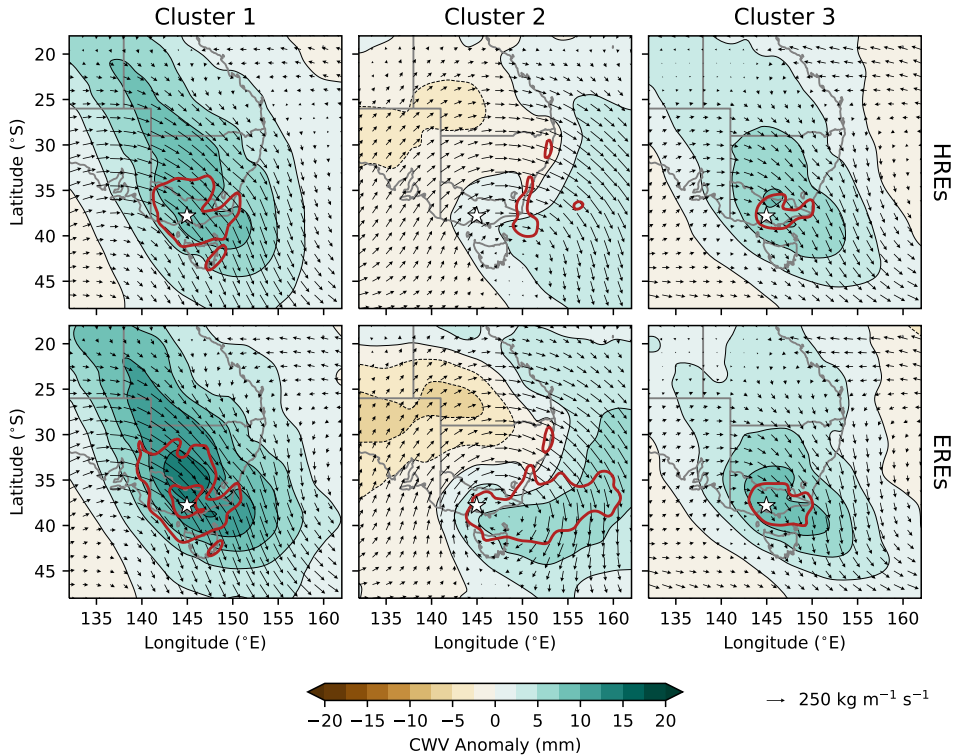


FIGURE 14 As in Fig. 10 but for each of the Melbourne clusters.

355 speeds around 5 kt stronger in EREs compared with HREs. This finding is again consistent with Callaghan and Power (2016),
 356 who found a strengthening of the easterlies at 700 hPa and an increase in the magnitude of the 850–500 hPa shear with increasing
 357 rainfall intensity in Brisbane (their Fig. 2). In contrast, for Melbourne the wind profiles for HREs and EREs are broadly similar,
 358 although Cluster 2 shows more pronounced cyclonic turning with height for extreme events (consistent with the more amplified
 359 upper-level pattern seen in Fig. 13).

360 To better summarise the characteristics of the atmospheric profiles, Fig. 16 shows box-and-whisker diagrams of various
 361 column-integrated diagnostics for HREs and EREs in each domain, both collectively (i.e. for all events, including those rejected
 362 from the clusters) and for each of the three clusters. For comparison, we also show the distribution for REs. To provide a cleaner
 363 distinction between the different tiers of events, EREs are excluded from the sample of HREs and HREs are excluded from the
 364 sample of REs. The diagnostics shown are CWV, column relative humidity (CRH), column-mean vertical velocity (\bar{w}), and a
 365 new quantity that we call the upward vapour transport (UVT). Each of these is computed between the surface and height z_t ,
 366 taken as the 100 hPa pressure level. Thus, CWV is given by

$$CWV = \int_0^{z_t} \rho q dz \quad (3)$$

367 where ρ is air density and q is specific humidity. This differs subtly from the gridded CWV analysed in the previous section,

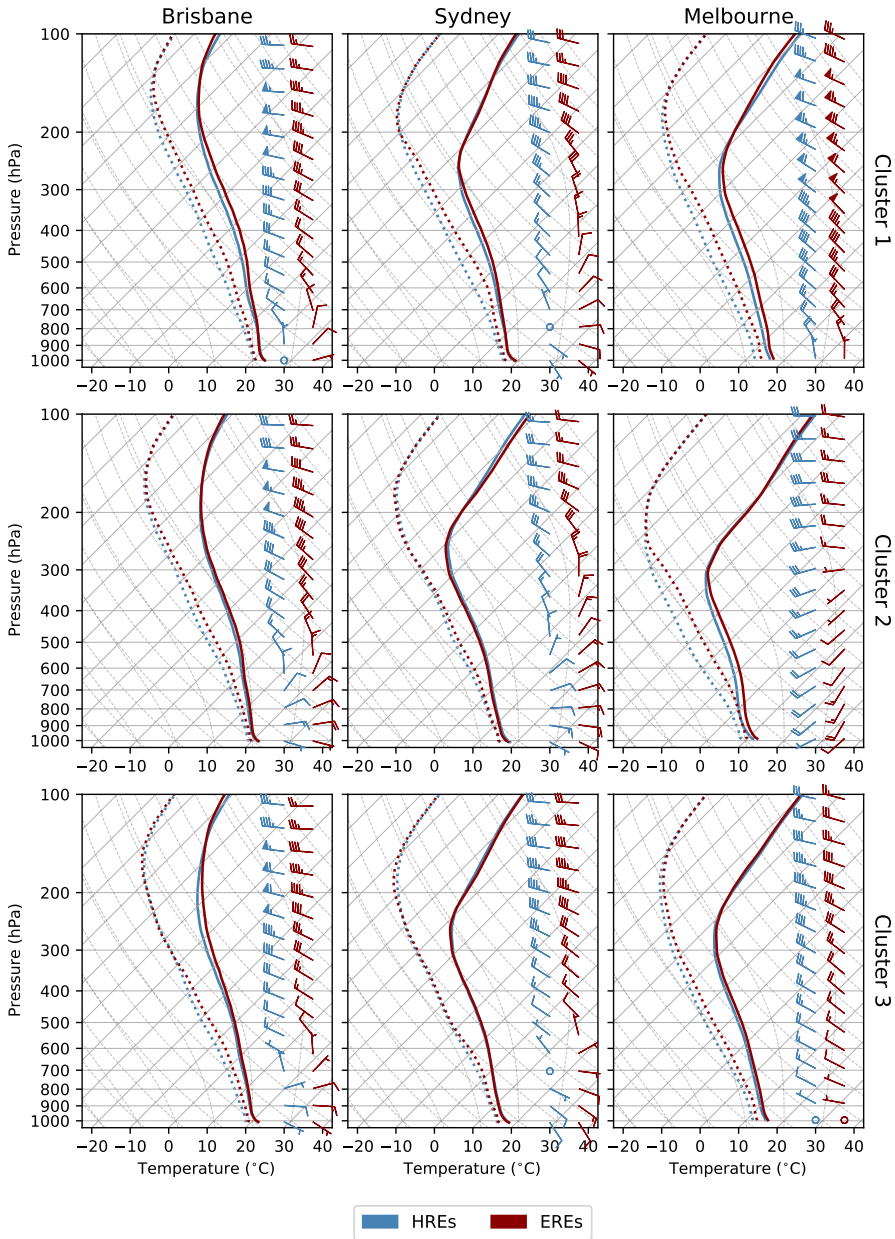


FIGURE 15 Skew- T -log- p diagrams showing composite profiles of temperature (solid lines), dewpoint temperature (dotted lines), and wind velocity (wind barbs, plotted every 1 km AGL; half barbs, full barbs, and pennants indicate speeds of 5, 10, and 50 knots, respectively) for HREs and EREs for each cluster in the (left to right) Brisbane, Sydney, and Melbourne domains.

368 which is a precomputed diagnostic in ERA5 based on an integral over the full column (up to the model top at 0.01 hPa). CRH,
 369 also known as the saturation fraction, is defined as the ratio of CWV to saturation CWV:

$$\text{CRH} = \frac{\int_0^{z_t} \rho q \, dz}{\int_0^{z_t} \rho q_{\text{sat}} \, dz}, \quad (4)$$

370 where q_{sat} is the saturation specific humidity. Note that saturation vapour pressure is computed with respect to water for
 371 temperatures above 0 °C and with respect to ice for temperatures below -23 °C, with a linear blending of the two between these
 372 temperatures (ECMWF 2016, section 7.4.2). Column-mean vertical velocity is computed as:

$$\bar{w} = \frac{1}{z_t} \int_0^{z_t} w \, dz, \quad (5)$$

373 where $w = -\omega/\rho g$ is the vertical velocity. We define UVT as as the column integral of the product of upward mass flux ρw_{U}
 374 ($w_{\text{U}} = w$ where $w > 0$ and $w_{\text{U}} = 0$ otherwise) and specific humidity:

$$\text{UVT} = \int_0^{z_t} \rho w_{\text{U}} q \, dz \quad (6)$$

375 Each of these quantities is computed using daily-mean (00–23 UTC) fields. Statistically significant differences between the
 376 distributions for EREs and OHREs, and those for OHREs and OREs, are defined using a Wilcoxon rank-sum test (Wilks 2011,
 377 chapter 5) with a 1 % test level, and indicated by asterisks in Fig. 16.

378 For CWV there is a clear increase in values going from REs to HREs to EREs across all three domains; however, the
 379 difference between heavy and extreme events is less pronounced and not statistically significant for Sydney. This may reflect
 380 a greater similarity in the seasonal distribution of HREs and EREs in Sydney compared to Brisbane and Melbourne (Fig. 5).
 381 As we would expect, for a given event type, CWV decreases as we move poleward; for example, for EREs the median value
 382 decreases from 47 mm in Brisbane, to 33 mm in Sydney, to just 25 mm in Melbourne. Comparing the different clusters, we see
 383 significant variability, particularly in Melbourne where the 90th percentile of the ERE distribution for Cluster 2 is less than the
 384 median for Clusters 1 and 3.

385 CRH shows arguably the clearest distinction between REs and HREs, with the 75th percentile of the RE distribution being
 386 less than the 25th percentile of the HRE distribution in all domains. A CRH threshold of around 70 % would seem to offer a
 387 fairly robust method for identifying HREs based on environmental data alone (at least in ERA5). Significant differences are also
 388 seen between heavy and extreme events across all domains and clusters, with a threshold of around 80 % separating the lower
 389 half of the HRE distribution from the upper three quarters of the ERE distribution in Brisbane and Sydney. For Melbourne this
 390 threshold is closer to 75 % and there is more overlap between the distributions.

391 For REs in all three domains, the distribution of \bar{w} is roughly symmetric and centred on zero, whereas heavy and extreme
 392 events are almost always characterised by column-mean ascent. Significant differences are generally found between the
 393 distributions for HREs and EREs (with the exception of Cluster 3 in Brisbane), although we again observe greater overlap in
 394 Melbourne.

395 Combining vertical velocity and moisture in the form of UVT provides the strongest separation between heavy and extreme
 396 events in Brisbane and Sydney. On the other hand, the HRE and ERE distributions for Melbourne show slightly more overlap for
 397 UVT compared to CWV. Nevertheless, statistically significant differences are found for all clusters, with the 25th percentile of
 398 the ERE distribution generally being greater than the median of the HRE distribution. On average, for Brisbane and Sydney,
 399 $\text{UVT} > 1 \text{ kg m}^{-1} \text{ s}^{-1}$ seems to represent an appropriate threshold for isolating EREs, while in Melbourne the optimum value is
 400 closer to $0.5 \text{ kg m}^{-1} \text{ s}^{-1}$, with greater overlap once again between the distributions.

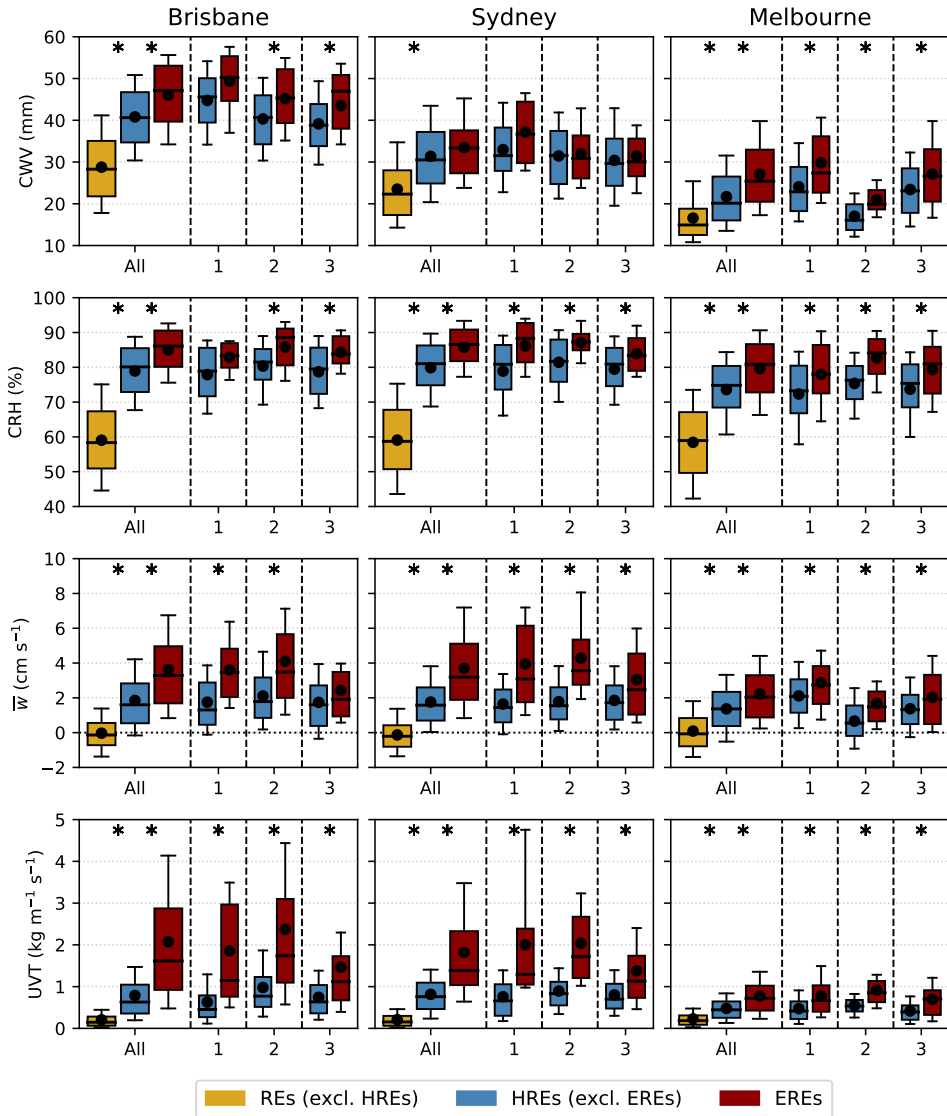


FIGURE 16 Box-and-whisker plots showing the distribution of (top to bottom) column water vapour (CWV), column relative humidity (CRH), column-mean vertical velocity (\bar{w}), and upward vapour transport (UVT), for REs (excluding HREs), HREs (excluding EREs), and EREs in the (left to right) Brisbane, Sydney, and Melbourne domains. Separate distributions are shown for all events (wide boxes) and each of the three clusters (narrow boxes). Boxes show the interquartile range, whiskers show the 10th and 90th percentiles, horizontal bars show the median, and filled circles show the mean. Asterisks at the top of each panel indicate where the difference between adjacent distributions is statistically significant at the 1 % level.

401 Numerous studies have sought to link short-duration (subdaily to daily) rainfall intensity to variations in surface air
 402 temperature, based on the Clausius–Clapeyron relationship between temperature and saturation vapour pressure (e.g. Lenderink

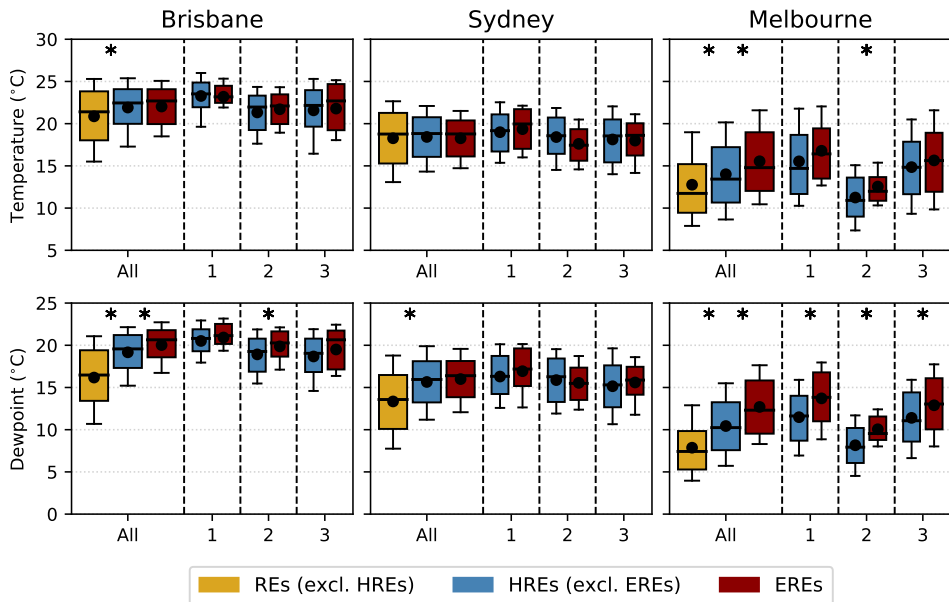


FIGURE 17 As in Fig. 16 but showing distributions of (top) 2 m temperature and (bottom) 2m dewpoint temperature.

and Van Meijgaard, 2008; Shaw et al., 2011; Molnar et al., 2015). Such scaling arguments are appealing due to their simplicity and because they can be used to infer future changes in precipitation extremes based on projections of surface temperature, which is much better constrained in climate models than precipitation. However, they neglect the possible two-way nature of the temperature–precipitation relationship (Ali and Mishra, 2017; Bao et al., 2017; Visser et al., 2020) as well as the role of humidity (Hardwick Jones et al., 2010; Prein et al., 2017), which can lead to counter-intuitive scaling rates (Utsumi et al., 2011; Maeda et al., 2012; Wang et al., 2017). To try to address these limitations, more recent studies have proposed using surface dewpoint instead of temperature (Barbero et al., 2018; Lenderink et al., 2018), which leads to more consistent scaling rates (Lenderink et al., 2011; Ali et al., 2018; Wasko et al., 2018; Zhang et al., 2019). However, this approach still neglects variations in moisture above the surface, as well as the critical role of circulation (e.g. Pfahl et al., 2017).

For comparison with these studies, the analysis presented in Fig. 16 was repeated using 2 m temperature and dewpoint temperature, both computed as daily (00–23 UTC) averages. Differences in the distribution of 2 m temperature (Fig. 17, top row) for REs, HREs, and EREs are only pronounced for Melbourne, consistent with the distinct seasonal distributions for the three event types (Fig. 5). In contrast, for both Brisbane and Sydney, the HRE and ERE distributions are contained entirely within the RE distribution. Furthermore, for some clusters (Cluster 1 in Brisbane and Cluster 2 in Sydney) the median temperature is actually lower for EREs than HREs. The results for 2 m dewpoint temperature (Fig. 17, bottom row) are very similar to those for CWV, with significant differences between the event types for all clusters in Melbourne and less pronounced differences for Brisbane and, in particular, Sydney. This is consistent with Bui et al. (2019) who found consistent precipitation scaling with dewpoint temperature at the surface and in various layers above the surface, based on station and radiosonde data in Australia. Overall, we see that while higher dewpoint temperatures are favourable for heavy and extreme rainfall, they do not represent a sufficient condition for these events. Instead anomalous moisture must coincide with large-scale ascent and a near-saturated column, allowing this moisture to be realised as precipitation.

CONCLUSIONS

This study has examined the characteristics of heavy rainfall events (HREs) and extreme rainfall events (EREs) in the major cities of Brisbane, Sydney, and Melbourne in southeast Australia. These events were defined by applying percentile thresholds (respectively, the 95th and 99th percentiles of rainfall ≥ 1 mm) to daily rain gauge observations over the 40-year period from 1979 to 2018. Two gauges, separated by at least 50 km, were required to meet the threshold in order to eliminate highly localised events. The large-scale circulation patterns (LSCPs) associated with HREs and EREs were explored by applying K-means clustering to gridded fields of the daily-mean standardised anomaly of mean sea-level pressure (MSLP) from ERA5. Three clusters were defined for each domain, with a minority (~5–10 %) of events assigned to a separate rejected category based on their dissimilarity to the cluster centroids. Composite synoptic maps and vertical profiles were produced for each cluster, separately for HREs and EREs, to highlight the key environmental ingredients for extreme rainfall. In addition, we explored the ability of the LSCPs and a range of environmental parameters to distinguish between ordinary, heavy, and extreme rainfall events.

Our main findings are as follows:

1. Although rare, HREs and EREs represent a significant contribution to total rainfall. For the majority of gauges in Brisbane and Sydney, the contribution from HREs exceeds 25 % and the contribution from EREs is at least 8 %. Values are slightly lower in Melbourne due to a higher frequency of light precipitation.
2. HREs occur predominantly in the warmer months in Brisbane and Sydney, but are more evenly distributed across the year in Melbourne. On the other hand, over half of Melbourne's EREs occur from November to February.
3. Multi-day HREs are more common in Brisbane and Sydney than in Melbourne, while in all three domains, EREs are more likely than HREs to be embedded in a multi-day event. Around a third of HREs and over half all EREs occur as part of a multi-day HRE in Brisbane and Sydney, whereas around a quarter of HREs and a third of EREs occur as part of a multi-day HRE in Melbourne. Multi-day EREs are rarer but still make up around a fifth of these events in each domain.
4. The LSCPs identified through cluster analysis all show a strong association with heavy and extreme rainfall. The probability of HREs and EREs is significantly enhanced (compared to climatology) for days where there is a strong correlation between the daily mean standardised MSLP anomaly and one of the cluster centroids. This is particularly true for Cluster 3 in Melbourne, which shows a five-fold increase in the probability of heavy and extreme rainfall for pattern correlations > 0.6 .
5. HREs in Brisbane and Sydney tend to be associated with a coastal trough/low, with an anomalous north-to-south pressure gradient driving moist air onshore from the Tasman and Coral Seas. In Melbourne, the LSCPs associated with HREs show more variety, with the three clusters characterised by a front, a cut-off low, and an inland trough. Common to events in all cities is an upper-level trough to the west, with large-scale ascent, positive column water vapour (CWV) anomalies, and strong integrated vapour transport (IVT) over the analysis domain.
6. Compared to HREs, EREs are characterised by a more amplified upper-level trough, with stronger vertical motion and larger CWV anomalies over the analysis domain. In Brisbane and Sydney, EREs also feature stronger and deeper onshore (easterly) flow, promoting larger IVT. In contrast wind profiles are quite similar for HREs and EREs in Melbourne.
7. Upward vapour transport (UVT; Eq. 6), which combines the key ingredients of moisture and large-scale ascent, provides good discrimination between HREs and EREs, particularly in Brisbane and Sydney. Both UVT and column relative humidity also provide good discrimination between HREs and ordinary rain events in all three cities. On the other hand, distributions of surface temperature show a large degree of overlap between different event types, particularly in Sydney and Brisbane.

In summary, our results serve to highlight the distinct LSCPs that give rise to heavy and extreme rainfall in Australia's three most populous cities, but also the common ingredients that favour these events. While the patterns associated with HREs may exist on more of a continuum than is suggested by the clustering results, there is a clear benefit in performing this intermediate

step before producing synoptic composites. It would be misleading to simply average across all HREs for a given domain, since this would smear out the distinct circulations apparent in Fig. 9–14. This is particularly true for Melbourne where the wave patterns for Clusters 1 and 2 are approximately 90° out of phase (Fig. 13), leading to near-orthogonal wind profiles (Fig. 15). Nevertheless, there are certain meteorological ingredients that are common to all events, irrespective of the LSCP. In particular, large CWV in the presence of upward vertical motion and a near-saturated column reflects a favourable combination of thermodynamics and dynamics for heavy and extreme rainfall.

A key limitation of our study is that HREs and EREs are defined based on daily (0900–0900 local time) rainfall accumulations. In reality the actual rainfall events will cover a range of time spans, with some lasting only a few hours and others persisting over several days (as indicated by Fig. 6). Multi-day events will likely be defined by persistent LSCPs and will therefore automatically receive a stronger weighting in the cluster analysis. Furthermore, some short-duration events may be missed if their rainfall happens to be split across two rain days. It would be valuable to repeat some of the analysis presented herein for HREs and EREs spanning different time scales, and to compare the environmental characteristics of short- and long-duration events. Identification of these events could make use of the recently developed Global Sub-Daily Rainfall dataset (Lewis et al., 2019) or gridded remote-sensing products such as IMERG (Integrated Multi-Satellite Retrievals for GPM; Tan et al., 2019). The latter permit the examination of rainfall extremes at a range of spatial scales (e.g. Zhou et al., 2019), but are subject to greater uncertainty in precipitation amounts due to limitations in the methods used to retrieve rain rates.

Future work will explore the characteristics of the precipitation systems that give rise to rainfall extremes in Australia using ground-based radar observations from the recently released Australian Radar Archive (<https://www.openradar.io/>). This dataset includes over 20 years of observations for some locations (including Brisbane, Sydney, and Melbourne), providing valuable information on the spatial extent, organisation, and lifecycle of precipitation systems. Other avenues for future work include high-resolution modelling studies to explore the mechanisms that govern extreme-rain-producing systems and an assessment of the ability of current-generation weather and climate models to capture these events and their associated circulation patterns. Ultimately, the knowledge gained from these studies should be used to inform model developments and refine forecasting paradigms, so that Australia can better cope with extreme events now and in the future.

ACKNOWLEDGEMENTS

This work was supported by the Australian Research Council through the Centre of Excellence for Climate Extremes (CLEX). Computational resources were provided by the National Computational Infrastructure (NCI), which is supported by the Australian Government. The authors thank Paola Petrelli for technical support with ERA5 and two anonymous reviewers for their feedback on an earlier draft of the manuscript.

REFERENCES

- Lisa V Alexander, Hayley J Fowler, Margot Bador, Ali Behrangi, Markus G Donat, Robert Dunn, Chris Funk, James Goldie, Elizabeth Lewis, Marine Rogé, et al. On the use of indices to study extreme precipitation on sub-daily and daily timescales. *Environmental Research Letters*, 14:125008, 2019.
- Haider Ali and Vimal Mishra. Contrasting response of rainfall extremes to increase in surface air and dewpoint temperatures at urban locations in India. *Scientific Reports*, 7:1–15, 2017.
- Haider Ali, Hayley J Fowler, and Vimal Mishra. Global observational evidence of strong linkage between dew point temperature and precipitation extremes. *Geophysical Research Letters*, 45:12320–12330, 2018.
- Richard P Allan, Stephen Blenkinsop, Hayley J Fowler, and Adrian J Champion. Atmospheric precursors for intense summer rainfall over the United Kingdom. *International Journal of Climatology*, 40:3849–3867, 2019.

- 503 Jiawei Bao, Steven C Sherwood, Lisa V Alexander, and Jason P Evans. Future increases in extreme precipitation exceed observed
504 scaling rates. *Nature Climate Change*, 7:128–132, 2017.
- 505 R Barbero, S Westra, G Lenderink, and HJ Fowler. Temperature-extreme precipitation scaling: A two-way causality? *International*
506 *Journal of Climatology*, 38:e1274–e1279, 2018.
- 507 Mitchell T Black and Todd P Lane. An improved diagnostic for summertime rainfall along the eastern seaboard of Australia. *International*
508 *Journal of Climatology*, 35:4480–4492, 2015.
- 509 Keith A Browning. Conceptual models of precipitation systems. *Weather and Forecasting*, 1:23–41, 1986.
- 510 Andrew Bui, Fiona Johnson, and Conrad Wasko. The relationship of atmospheric air temperature and dew point temperature to extreme
511 rainfall. *Environmental Research Letters*, 14:074025, 2019.
- 512 Jeff Callaghan and Scott B Power. Major coastal flooding in southeastern Australia 1860–2012, associated deaths and weather systems.
513 *Australian Meteorological and Oceanographic Journal*, 64:183–213, 2014.
- 514 Jeff Callaghan and Scott B Power. A vertical wind structure that leads to extreme rainfall and major flooding in southeast Australia.
515 *Journal of Southern Hemisphere Earth System Science*, 66:380–401, 2016.
- 516 Jennifer Louise Catto and S Pfahl. The importance of fronts for extreme precipitation. *Journal of Geophysical Research: Atmospheres*,
517 118:10–791, 2013.
- 518 Leone Cavicchia, Acacia Pepler, Andrew Dowdy, and Kevin Walsh. A physically based climatology of the occurrence and intensification
519 of Australian east coast lows. *Journal of Climate*, 32:2823–2841, 2019.
- 520 Adrian J Champion, Stephen Blenkinsop, Xiao-Feng Li, and Hayley J Fowler. Synoptic-scale precursors of extreme UK summer
521 3-hourly rainfall. *Journal of Geophysical Research: Atmospheres*, 124:4477–4489, 2019.
- 522 Yang Chen and Panmao Zhai. Two types of typical circulation pattern for persistent extreme precipitation in Central–Eastern China.
523 *Quarterly Journal of the Royal Meteorological Society*, 140:1467–1478, 2014.
- 524 Thomas H Chubb, Steven T Siems, and Michael J Manton. On the decline of wintertime precipitation in the Snowy Mountains of
525 southeastern Australia. *Journal of Hydrometeorology*, 12:1483–1497, 2011.
- 526 Steefan Contractor, Lisa V Alexander, Markus G Donat, and Nicholas Herold. How well do gridded datasets of observed daily precipi-
527 tation compare over Australia? *Advances in Meteorology*, 2015:1–15, 2015.
- 528 Andries Jan de Vries, Huug G Ouwersloot, Steven B Feldstein, Michael Riemer, Ahmed M El Kenawy, Matthew F McCabe, and Jos
529 Lelieveld. Identification of tropical-extratropical interactions and extreme precipitation events in the Middle East based on potential
530 vorticity and moisture transport. *Journal of Geophysical Research: Atmospheres*, 123:861–881, 2018.
- 531 DP Dee, SM Uppala, AJ Simmons, P Berrisford, P Poli, S Kobayashi, U Andrae, MA Balmaseda, G Balsamo, P Bauer, P Bechtold, ACM
532 Beljaars, L van de Berg, J Bidlot, N Bormann, C Delsol, R Dragani, M Fuentes, AJ Geer, L Haimberger, SB Healy, H Hersbach,
533 EV Hólm, L Isaksen, P Kållberg, M Köhler, M Matricardi, AP McNally, BM Monge-Sanz, J-J Morcrette, B-K Park, C Peubey,
534 P de Rosnay, C Tavolato, J-N Thépaut, and F Vitart. The ERA-Interim reanalysis: Configuration and performance of the data
535 assimilation system. *Quarterly Journal of the Royal Meteorological Society*, 137:553–597, 2011.
- 536 Andrew J Dowdy and Jennifer L Catto. Extreme weather caused by concurrent cyclone, front and thunderstorm occurrences. *Scientific*
537 *Reports*, 7:40359, 2017.
- 538 Andrew J Dowdy, Acacia Pepler, Alejandro Di Luca, Leone Cavicchia, Graham Mills, Jason P Evans, Simon Louis, Kathleen L McInnes,
539 and Kevin Walsh. Review of Australian east coast low pressure systems and associated extremes. *Climate Dynamics*, 53:4887–4910,
540 2019.
- 541 ECMWF. Part IV: Physical Processes. In *IFS Documentation – Cy43r1*. European Centre for Medium Range Weather Forecasts, 2016.
542 Available online at <https://www.ecmwf.int/sites/default/files/elibrary/2016/17117-part-iv-physical-processes.pdf>.

- 543 Sonya Louise Fiddes, Alexandre Bernardes Pezza, and Vaughan Barras. Synoptic climatology of extreme precipitation in alpine Aus-
544 tralia. *International Journal of Climatology*, 35:172–188, 2015.
- 545 Federico Grazzini, George C Craig, Christian Keil, Gabriele Antolini, and Valentina Pavan. Extreme precipitation events over northern
546 Italy. Part I: A systematic classification with machine-learning techniques. *Quarterly Journal of the Royal Meteorological Society*,
547 146:69–85, 2020.
- 548 Rhys Hardwick Jones, Seth Westra, and Ashish Sharma. Observed relationships between extreme sub-daily precipitation, surface
549 temperature, and relative humidity. *Geophysical Research Letters*, 37:L22805, 2010.
- 550 Seraphine Hauser, Christian M Grams, Michael J Reeder, Shayne McGregor, Andreas H Fink, and Julian F Quinting. A weather
551 system perspective on winter–spring rainfall variability in southeastern Australia during El Niño. *Quarterly Journal of the Royal
552 Meteorological Society*, 146:2614–2633, 2020.
- 553 Hans Hersbach, Bill Bell, Paul Berrisford, Shoji Hirahara, András Horányi, Joaquín Muñoz-Sabater, Julien Nicolas, Carole Peubey,
554 Raluca Radu, Dinand Schepers, Adrian Simmons, Cornel Soci, Saleh Abdalla, Xavier Abellan, Gianpaolo Balsamo, Peter Bechtold,
555 Gionata Biavati, Jean Bidlot, Massimo Bonavita, Giovanna Chiara, Per Dahlgren, Dick Dee, Michail Diamantakis, Rossana Dragani,
556 Johannes Flemming, Richard Forbes, Manuel Fuentes, Alan Geer, Leo Haimberger, Sean Healy, Robin J Hogan, Elías Hólm, Marta
557 Janisková, Sarah Keeley, Patrick Laloyaux, Philippe Lopez, Cristina Lupu, Gabor Radnoti, Patricia Rosnay, Iryna Rozum, Freja
558 Vamborg, Sebastien Villaume, and Jean-Noël Thépaut. The ERA5 global reanalysis. *Quarterly Journal of the Royal Meteorological
559 Society*, 146:1999–2049, 2020.
- 560 CM Holgate, JP Evans, AIJM Van Dijk, AJ Pitman, and G Di Virgilio. Australian precipitation recycling and evaporative source regions.
561 *Journal of Climate*, 33:8721–8735, 2020.
- 562 Greg J Holland, Amanda H Lynch, and Lance M Leslie. Australian east-coast cyclones. Part I: Synoptic overview and case study.
563 *Monthly Weather Review*, 115:3024–3036, 1987.
- 564 EE Houssos, CJ Lolis, and A Bartzokas. Atmospheric circulation patterns associated with extreme precipitation amounts in Greece.
565 *Advances in Geosciences*, 17:5–11, 2008.
- 566 Yang Hu, Yi Deng, Zhimin Zhou, Chunguang Cui, and Xiquan Dong. A statistical and dynamical characterization of large-scale
567 circulation patterns associated with summer extreme precipitation over the middle reaches of Yangtze river. *Climate Dynamics*, 52:
568 6213–6228, 2019.
- 569 Ling Huang, Yali Luo, and Da-Lin Zhang. The relationship between anomalous presummer extreme rainfall over South China and
570 synoptic disturbances. *Journal of Geophysical Research: Atmospheres*, 123:3395–3413, 2018.
- 571 Robert Huva, Roger Dargaville, and Peter Rayner. The impact of filtering self-organizing maps: a case study with Australian pressure
572 and rainfall. *International Journal of Climatology*, 35:624–633, 2014.
- 573 David A Jones, William Wang, and Robert Fawcett. High-quality spatial climate data-sets for Australia. *Australian Meteorological and
574 Oceanographic Journal*, 58:233–248, 2009.
- 575 Youichi Kamae, Wei Mei, and Shang-Ping Xie. Climatological relationship between warm season atmospheric rivers and heavy rainfall
576 over East Asia. *Journal of the Meteorological Society of Japan*, 95:411–431, 2017.
- 577 Andrew D King, Lisa V Alexander, and Markus G Donat. The efficacy of using gridded data to examine extreme rainfall characteristics:
578 a case study for Australia. *International Journal of Climatology*, 33:2376–2387, 2013.
- 579 Andrew D King, Nicholas P Klingaman, Lisa V Alexander, Markus G Donat, Nicolas C Jourdain, and Penelope Maher. Extreme rainfall
580 variability in Australia: patterns, drivers, and predictability. *Journal of Climate*, 27:6035–6050, 2014.
- 581 Andrew D King, Debra Hudson, Eun-Pa Lim, Andrew G Marshall, Harry H Hendon, Todd P Lane, and Oscar Alves. Sub-seasonal to
582 seasonal prediction of rainfall extremes in Australia. *Quarterly Journal of the Royal Meteorological Society*, 160:2228–2249, 2020.

- 583 David B Knight and Robert E Davis. Contribution of tropical cyclones to extreme rainfall events in the southeastern United States.
584 *Journal of Geophysical Research: Atmospheres*, 114:D23102, 2009.
- 585 Charles E Konrad. Synoptic-scale features associated with warm season heavy rainfall over the interior southeastern United States.
586 *Weather and Forecasting*, 12:557–571, 1997.
- 587 David A Lavers, Richard P Allan, Eric F Wood, Gabriele Villarini, David J Brayshaw, and Andrew J Wade. Winter floods in Britain are
588 connected to atmospheric rivers. *Geophysical Research Letters*, 38:L23803, 2011.
- 589 G Lenderink, HY Mok, TC Lee, and GJ Van Oldenborgh. Scaling and trends of hourly precipitation extremes in two different climate
590 zones-Hong Kong and the Netherlands. *Hydrology and Earth System Sciences*, 15:3033–3041, 2011.
- 591 Geert Lenderink and Erik Van Meijgaard. Increase in hourly precipitation extremes beyond expectations from temperature changes.
592 *Nature Geoscience*, 1:511–514, 2008.
- 593 Geert Lenderink, Renaud Barbero, Seth Westra, and Hayley J Fowler. Reply to comments on “Temperature-extreme precipitation
594 scaling: A two-way causality?”. *International Journal of Climatology*, 38:4664–4666, 2018.
- 595 Elizabeth Lewis, Hayley Fowler, Lisa Alexander, Robert Dunn, Fergus McClean, Renaud Barbero, Selma Guerreiro, Xiao-Feng Li, and
596 Stephen Blenkinsop. GSDR: a global sub-daily rainfall dataset. *Journal of Climate*, 32:4715–4729, 2019.
- 597 Robert A Maddox, Charles F Chappell, and Lee R Hoxit. Synoptic and meso- α scale aspects of flash flood events. *Bulletin of the
598 American Meteorological Society*, 60:115–123, 1979.
- 599 Eduardo Eiji Maeda, Nobuyuki Utsumi, and Taikan Oki. Decreasing precipitation extremes at higher temperatures in tropical regions.
600 *Natural Hazards*, 64:935–941, 2012.
- 601 Olivia Martius, Evelyn Zenklusen, Cornelia Schwierz, and Huw C Davies. Episodes of Alpine heavy precipitation with an overlying
602 elongated stratospheric intrusion: A climatology. *International Journal of Climatology: A Journal of the Royal Meteorological
603 Society*, 26:1149–1164, 2006.
- 604 Matthew J Menne, Imke Durre, Russell S Vose, Byron E Gleason, and Tamara G Houston. An overview of the global historical
605 climatology network-daily database. *Journal of Atmospheric and Oceanic Technology*, 29:897–910, 2012.
- 606 Seung-Ki Min, Wenju Cai, and Penny Whetton. Influence of climate variability on seasonal extremes over Australia. *Journal of
607 Geophysical Research: Atmospheres*, 118:643–654, 2013.
- 608 Peter Molnar, Simone Faticchi, Ladislav Gaál, Jan Szolgay, and Paolo Burlando. Storm type effects on super Clausius–Clapeyron scaling
609 of intense rainstorm properties with air temperature. *Hydrology and Earth System Sciences*, 19:1753, 2015.
- 610 Benjamin J Moore, Daniel Keyser, and Lance F Bosart. Linkages between extreme precipitation events in the central and eastern United
611 States and Rossby wave breaking. *Monthly Weather Review*, 147:3327–3349, 2019.
- 612 Neville Nicholls, Wasyl Drosdowsky, and Beth Lavery. Australian rainfall variability and change. *Weather*, 52:66–72, 1997.
- 613 O Nuissier, B Joly, A Joly, V Ducrocq, and P Arbogast. A statistical downscaling to identify the large-scale circulation patterns
614 associated with heavy precipitation events over southern France. *Quarterly Journal of the Royal Meteorological Society*, 137:
615 1812–1827, 2011.
- 616 Masamichi Ohba, Shinji Kadokura, Yoshikatsu Yoshida, Daisuke Nohara, and Yasushi Toyoda. Anomalous weather patterns in relation
617 to heavy precipitation events in Japan during the Baiu season. *Journal of Hydrometeorology*, 16:688–701, 2015.
- 618 F Pedregosa, G Varoquaux, A Gramfort, V Michel, B Thirion, O Grisel, M Blondel, P Prettenhofer, R Weiss, V Dubourg, J Vanderplas,
619 A Passos, D Cournapeau, M Brucher, M Perrot, and E Duchesnay. Scikit-learn: Machine learning in Python. *Journal of Machine
620 Learning Research*, 12:2825–2830, 2011.

- 621 Angeline G Pendergrass and Reto Knutti. The uneven nature of daily precipitation and its change. *Geophysical Research Letters*, 45:
622 11980–11988, 2018.
- 623 Acacia Pepler, Aaron Coutts-Smith, and Bertrand Timbal. The role of East Coast Lows on rainfall patterns and inter-annual variability
624 across the East Coast of Australia. *International Journal of Climatology*, 34:1011–1021, 2014.
- 625 Acacia S Pepler, Alejandro Di Luca, Fei Ji, Lisa V Alexander, Jason P Evans, and Steven C Sherwood. Impact of identification method
626 on the inferred characteristics and variability of Australian East Coast Lows. *Monthly Weather Review*, 143:864–877, 2015.
- 627 Acacia S Pepler, Andrew J Dowdy, Peter van Rensch, Irina Rudeva, Jennifer L Catto, and Pandora Hope. The contributions of fronts,
628 lows and thunderstorms to southern Australian rainfall. *Climate Dynamics*, 55:1489–1505, 2020.
- 629 Stephan Pfahl and Heini Wernli. Quantifying the relevance of cyclones for precipitation extremes. *Journal of Climate*, 25:6770–6780,
630 2012.
- 631 Stephan Pfahl, Paul A O’Gorman, and Erich M Fischer. Understanding the regional pattern of projected future changes in extreme
632 precipitation. *Nature Climate Change*, 7:423–427, 2017.
- 633 Guy Plaut, Evi Schuepbach, and Marut Doctor. Heavy precipitation events over a few Alpine sub-regions and the links with large-scale
634 circulation, 1971–1995. *Climate Research*, 17:285–302, 2001.
- 635 Michael J Pook, Peter C McIntosh, and Gary A Meyers. The synoptic decomposition of cool-season rainfall in the southeastern
636 Australian cropping region. *Journal of Applied Meteorology and Climatology*, 45:1156–1170, 2006.
- 637 Andreas F Prein, Roy M Rasmussen, Kyoko Ikeda, Changhai Liu, Martyn P Clark, and Greg J Holland. The future intensification of
638 hourly precipitation extremes. *Nature Climate Change*, 7:48–52, 2017.
- 639 F Martin Ralph, Paul J Neiman, Gary A Wick, Seth I Gutman, Michael D Dettinger, Daniel R Cayan, and Allen B White. Flooding on
640 California’s Russian River: Role of atmospheric rivers. *Geophysical Research Letters*, 33:L13801, 2006.
- 641 Markus Rau, Yi He, Clare Goodess, and András Bárdossy. Statistical downscaling to project extreme hourly precipitation over the
642 United Kingdom. *International Journal of Climatology*, 40:1805–1823, 2020.
- 643 Kimberley J Reid, Ian Simmonds, Claire L Vincent, and Andrew D King. The Australian Northwest Cloudband: Climatology, Mecha-
644 nisms, and Association with Precipitation. *Journal of Climate*, 32:6665–6684, 2019.
- 645 James S Risbey, Michael J Pook, Peter C McIntosh, Matthew C Wheeler, and Harry H Hendon. On the remote drivers of rainfall
646 variability in Australia. *Monthly Weather Review*, 137:3233–3253, 2009.
- 647 James S Risbey, Peter C McIntosh, and Michael J Pook. Synoptic components of rainfall variability and trends in southeast Australia.
648 *International Journal of Climatology*, 33:2459–2472, 2013.
- 649 Stephen B Shaw, A Alisa Royem, and Susan J Riha. The relationship between extreme hourly precipitation and surface temperature in
650 different hydroclimatic regions of the United States. *Journal of Hydrometeorology*, 12:319–325, 2011.
- 651 Milton Speer and Bart Geerts. A synoptic–mesoalpha-scale climatology of flash-floods in the Sydney metropolitan area. *Australian
652 Meteorological Magazine*, 43:87–103, 1994.
- 653 Milton S Speer, Perry Wiles, and Acacia Pepler. Low pressure systems off the New South Wales coast and associated hazardous weather:
654 establishment of a database. *Australian Meteorological and Oceanographic Journal*, 58:29–39, 2009.
- 655 Dustin Swales, Mike Alexander, and Mimi Hughes. Examining moisture pathways and extreme precipitation in the US Intermountain
656 West using self-organizing maps. *Geophysical Research Letters*, 43:1727–1735, 2016.
- 657 Jackson Tan, George J Huffman, David T Bolvin, and Eric J Nelkin. IMERG V06: Changes to the morphing algorithm. *Journal of
658 Atmospheric and Oceanic Technology*, 36:2471–2482, 2019.

- 659 CR Tozer, AS Kiem, and DC Verdon-Kidd. On the uncertainties associated with using gridded rainfall data as a proxy for observed.
660 *Hydrology and Earth System Sciences*, 16:1481, 2012.
- 661 SM Uppala, PW Kållberg, AJ Simmons, U Andrae, V Da Costa Bechtold, M Fiorino, JK Gibson, J Haseler, A Hernandez, GA Kelly,
662 X Li, K Onogi, S Saarinen, N Sokka, RP Allan, E Andersson, K Arpe, MA Balmaseda, ACM Beljaars, L Van De Berg, J Bidlot,
663 N Bormann, S Caires, F Chevallier, A Dethof, M Dragosavac, M Fisher, M Fuentes, S Hagemann, E Hólm, BJ Hoskins, I Isaksen,
664 PAEM Janssen, R Jenne, AP McNally, J-F Mahfouf, J-J Morcrette, NA Rayner, RW Saunders, P Simon, A Sterl, KE Trenberth,
665 A Untch, D Vasiljevic, P Viterbo, and J Woollen. The ERA-40 re-analysis. *Quarterly Journal of the Royal Meteorological Society*,
666 131:2961–3012, 2005.
- 667 Nobuyuki Utsumi, Shinta Seto, Shinjiro Kanae, Eduardo Eiji Maeda, and Taikan Oki. Does higher surface temperature intensify extreme
668 precipitation? *Geophysical Research Letters*, 38:L16708, 2011.
- 669 Nobuyuki Utsumi, Hyungjun Kim, Shinjiro Kanae, and Taikan Oki. Relative contributions of weather systems to mean and extreme
670 global precipitation. *Journal of Geophysical Research: Atmospheres*, 122:152–167, 2017.
- 671 Gabriele Villarini and Rhawn F Denniston. Contribution of tropical cyclones to extreme rainfall in Australia. *International Journal of*
672 *Climatology*, 36:1019–1025, 2016.
- 673 JB Visser, C Wasko, A Sharma, and R Nathan. Resolving inconsistencies in extreme precipitation-temperature sensitivities. *Geophysical*
674 *Research Letters*, 47:e2020GL089723, 2020.
- 675 Guiling Wang, Dagang Wang, Kevin E Trenberth, Amir Erfanian, Miao Yu, Michael G Bosilovich, and Dana T Parr. The peak structure
676 and future changes of the relationships between extreme precipitation and temperature. *Nature Climate Change*, 7:268–274, 2017.
- 677 Conrad Wasko, William Tang Lu, and Rajeshwar Mehrotra. Relationship of extreme precipitation, dry-bulb temperature, and dew point
678 temperature across Australia. *Environmental Research Letters*, 13:074031, 2018.
- 679 Daniel S Wilks. *Statistical Methods in the Atmospheric Sciences*. Academic Press, 3rd edition, 2011.
- 680 Qiang Zhang, Xihui Gu, Jianfeng Li, Peijun Shi, and Vijay P Singh. The impact of tropical cyclones on extreme precipitation over
681 coastal and inland areas of China and its association to ENSO. *Journal of Climate*, 31:1865–1880, 2018.
- 682 Wei Zhang, Gabriele Villarini, and Michael Wehner. Contrasting the responses of extreme precipitation to changes in surface air and
683 dew point temperatures. *Climatic Change*, 154:257–271, 2019.
- 684 Yaping Zhou, Kevin Nelson, Karen I Mohr, George J Huffman, Robert Levy, and Mircea Grecu. A Spatial-Temporal Extreme Precipitation
685 Database from GPM IMERG. *Journal of Geophysical Research: Atmospheres*, 124:10344–10363, 2019.